Strongly coupled interaction between a ridge of fluid and an inviscid airflow

C. Paterson, S. K. Wilson, and B. R. Duffy

Citation: Physics of Fluids **27**, 072104 (2015); doi: 10.1063/1.4926623
View online: http://dx.doi.org/10.1063/1.4926623
View Table of Contents: http://scitation.aip.org/content/aip/journal/pof2/27/7?ver=pdfcov
Published by the AIP Publishing

PHYSICS OF FLUIDS **27**, 072104 (2015)

Strongly coupled interaction between a ridge of fluid and an inviscid airflow

C. Paterson, S. K. Wilson,[a] and B. R. Duffy[b]
Department of Mathematics and Statistics, University of Strathclyde, Livingstone Tower, 26 Richmond Street, Glasgow G1 1XH, United Kingdom

(Received 19 March 2015; accepted 29 June 2015; published online 28 July 2015)

The behaviour of a steady thin sessile or pendent ridge of fluid on an inclined planar substrate which is strongly coupled to the external pressure gradient arising from an inviscid airflow parallel to the substrate far from the ridge is described. When the substrate is nearly horizontal, a very wide ridge can be supported against gravity by capillary and/or external pressure forces; otherwise, only a narrower (but still wide) ridge can be supported. Classical thin-aerofoil theory is adapted to obtain the governing singular integro-differential equation for the profile of the ridge in each case. Attention is focused mainly on the case of a very wide sessile ridge. The effect of strengthening the airflow is to push a pinned ridge down near to its edges and to pull it up near to its middle. At a critical airflow strength, the upslope contact angle reaches the receding contact angle at which the upslope contact line de-pins, and continuing to increase the airflow strength beyond this critical value results in the de-pinned ridge becoming narrower, thicker, and closer to being symmetric in the limit of a strong airflow. The effect of tilting the substrate is to skew a pinned ridge in the downslope direction. Depending on the values of the advancing and receding contact angles, the ridge may first de-pin at either the upslope or the downslope contact line but, in general, eventually both contact lines de-pin. The special cases in which only one of the contact lines de-pins are also considered. It is also shown that the behaviour of a very wide pendent ridge is qualitatively similar to that of a very wide sessile ridge, while the important qualitative difference between the behaviour of a very wide ridge and a narrower ridge is that, in general, for the latter one or both of the contact lines may never de-pin. © *2015 AIP Publishing LLC.*
[http://dx.doi.org/10.1063/1.4926623]

I. INTRODUCTION

The behaviour of a thin layer or droplet of viscous fluid in the presence of an airflow has been the subject of much theoretical and experimental research because of the many practically important situations in which it occurs (see, for example, Fan *et al.*[1]). In civil engineering, the interaction between the rivulets of rainwater that can form on the cables of cable-stayed bridges and the wind blowing past them is believed to play a crucial role in the rain–wind-induced vibrations of the cables (see, for example, Robertson *et al.*[2] and Lemaitre *et al.*[3]). In the electronics industry, a jet of air is sometimes used to remove droplets of water left on the surface of silicon wafers during the manufacture of microchips (see, for example, Kim *et al.*[4]). In the nuclear industry, careful control of the dry-out point at which the layer of water that forms on the inside surface of a steam-generating boiler pipe (through which both gas and vapour flow) completely vaporises is important for safe and efficient reactor operation (see, for example, Cuminato *et al.*[5]). Other areas in which a thin layer or droplet of fluid may be subject to an airflow include air-knife and spin-coating processes in industry (see, for example, Chou and Wu[6]) and in ice-accretion on aircraft (see, for example, Myers and Charpin[7]).

[a]Author to whom correspondence should be addressed. Electronic mail: s.k.wilson@strath.ac.uk
[b]Electronic mail: b.r.duffy@strath.ac.uk

In many situations the viscosity of the airflow plays an important role, and hence there is a considerable body of work, notably that by Li and Pozrikidis,[8] Dimitrakopoulos and Higdon,[9–12] Schleizer and Bonnecaze,[13] Yon and Pozrikidis,[14] Spelt,[15] Zhang *et al.*,[16] Dimitrakopoulos,[17,18] Ding and Spelt,[19] Shirani and Masoomi,[20] Sugiyama and Sbragaglia,[21] Ding *et al.*,[22] and Hao and Cheng,[23] using a variety of analytical and numerical methods to obtain considerable insight into the behaviour at low and moderate Reynolds numbers. In the present complementary contribution we adopt a semi-analytical approach based on classical thin-aerofoil theory to address the opposite extreme of high Reynolds number in which the viscosity of the airflow is negligible. Specifically, we formulate and analyse a singular integro-differential equation for the profile of a thin sessile or pendent ridge of fluid (or, equivalently, a two-dimensional droplet) on an inclined planar substrate which we solve numerically and asymptotically in appropriate limits. This approach is similar in spirit to, but very different in detail from, that of Sullivan *et al.*,[24] in which we used lubrication theory to analyse three closely related problems involving a thin ridge or rivulet of viscous fluid subject to a prescribed uniform transverse shear stress due to an airflow. However, one key difference between these two contributions is that while in the former work the effect of the airflow is idealised as a prescribed uniform shear stress which is independent of the shape of the ridge or rivulet, in the present work it is idealised as the non-uniform pressure distribution due to an inviscid airflow which is strongly coupled to the shape of the ridge.

We are not the first authors to use classical thin-aerofoil theory to tackle problems of this kind. Durbin[25] used thin-aerofoil theory to study the steady flow of a thin ridge on a horizontal substrate. Unlike in the present work, he assumed that the airflow detaches at some point on the free surface of the ridge resulting in an asymmetric ridge profile. Durbin[25] studied the critical case in which the strength of the airflow is at the maximum value such that the ridge is deformed but for which the contact lines do not de-pin. King and Tuck[26] used thin-aerofoil theory to study the steady flow of a thin ridge on an inclined substrate. Unlike in the present work, they included a constant shear stress at the free surface of the ridge due to the airflow, but neglected surface tension except near to the contact lines. King and Tuck[26] found that for each value of the angle of inclination of the substrate, there are zero, one, or two values of the strength of the airflow for which a steady solution exists. Subsequently, King *et al.*[27] used a similar approach to study steady surface waves on a layer of fluid flowing down an inclined substrate in the absence of surface tension. Cuminato *et al.*[5] used thin-aerofoil theory to study the steady flow of a thin layer on a heated horizontal substrate as a model for dry-out within a steam-generating boiler pipe. Unlike in the present work, they included both a constant shear stress at the free surface of the layer and evaporative mass loss from the layer, but neglected surface tension, and, in particular, calculated the location of the dry-out point.

In each of the studies mentioned above, using thin-aerofoil theory leads to a singular integro-differential equation for the unknown free surface profile of the fluid. Making analytical progress with this type of equation is not easy and techniques for solving them numerically are not routine. Instead, they must be treated on a problem-by-problem basis depending on the specific properties of the equation in each case, as described in the review by Cuminato *et al.*[28] on both linear and nonlinear singular integral and integro-differential equations arising in a wide variety of physical contexts.

There have, of course, also been many other studies in which the pressure gradient and/or the shear stress on a thin film of fluid due to an airflow is prescribed rather than being coupled to the unknown free surface profile (see, for example,[29–43]), but these are less directly relevant to the present strongly coupled problem.

The structure of the present work is as follows. In Sec. II we use a thin-film approximation to describe the behaviour of a steady thin sessile or pendent ridge of fluid on an inclined planar substrate, including the effects of gravity and surface tension, which is strongly coupled to the external pressure gradient arising from an inviscid airflow parallel to the substrate far from the ridge, and obtain the governing singular integro-differential equations for the profile of a very wide sessile ridge on a nearly horizontal substrate, a very wide pendent ridge on a nearly horizontal substrate, and a narrower (but still wide) sessile or pendent ridge. Our attention is focused mainly on the first of these problems. In Sec. III we describe some basic properties of the solution, while in Secs. IV and V we use a combination of numerical and asymptotic techniques to analyse the effect of varying the strength of the airflow and the angle of inclination of the substrate, respectively. Situations in which the contact lines

are pinned and in which one or both of the contact lines de-pin are considered. The behaviour of the ridge in the other two problems is somewhat similar to that in the first one, and so in Secs. VI and VII we consider these two problems only briefly, highlighting the qualitative similarities and differences between them and the first problem. Finally, in Sec. VIII we summarise the results obtained.

II. PROBLEM FORMULATION

Consider a steady thin sessile or pendent ridge of fluid (or, equivalently, a two-dimensional droplet) on a planar substrate inclined at an angle α ($0 \le \alpha \le \pi$) to the horizontal, in the presence of a steady inviscid airflow. Values of α satisfying $0 \le \alpha < \pi/2$ correspond to a sessile ridge sitting on an inclined substrate as sketched in Figure 1, values of α satisfying $\pi/2 < \alpha \le \pi$ correspond to a pendent ridge hanging from an inclined substrate. The values $\alpha = 0, \pi$ and $\alpha = \pi/2$ correspond to the special cases of a ridge on a horizontal and on a vertical substrate, respectively. We assume that the fluid in the ridge has constant density ρ and coefficient of surface tension σ, and that the ridge is subject to an airflow of constant density ρ_a parallel to the substrate far from the ridge with constant speed U_∞ and ambient pressure p_∞. The airflow is perturbed by the presence of the ridge, resulting in a non-uniform external pressure gradient that depends in a non-trivial way on the unknown free surface profile of the ridge. Referred to Cartesian coordinates Oxy with the x and y directions taken to be parallel and normal to the substrate, respectively, as indicated in Figure 1, the ridge has free surface profile $y = h(x)$ for $0 \le x \le L$, width L in the transverse (i.e., in the x) direction, prescribed constant volume per unit length in the longitudinal (i.e., in the z) direction V, maximum thickness $h = h_m$ at $x = x_m$, and downslope and upslope contact angles $\theta_1 = h'(0)$ (≥ 0) and $\theta_2 = -h'(L)$ (≥ 0), respectively. The pressure in both the air and the ridge is denoted by $p = p(x, y)$.

We introduce the following non-dimensionalised and scaled variables:

$$x = L_0 x^*, \quad x_m = L_0 x_m^*, \quad L = L_0 L^*, \quad h = \epsilon L_0 h^*, \quad h_m = \epsilon L_0 h_m^*, \quad V = \epsilon L_0^2 V^*, \tag{1}$$

together with

$$y = \epsilon L_0 y^*, \quad p - p_\infty = \frac{\epsilon\sigma}{L_0} p^* \quad \text{in the ridge,} \tag{2}$$

and

$$y = L_0 Y^*, \quad p - p_\infty = \frac{\epsilon\sigma}{L_0} P^* \quad \text{in the air,} \tag{3}$$

where L_0 is the characteristic transverse length scale (discussed in more detail below) and $\epsilon = V/L_0^2 \ll 1$ is the (small) transverse aspect ratio of the ridge, giving $V^* = 1$ without loss of generality. Hence in what follows we set $V^* = 1$ in all of the numerical calculations, but retain V^* explicitly in all of the

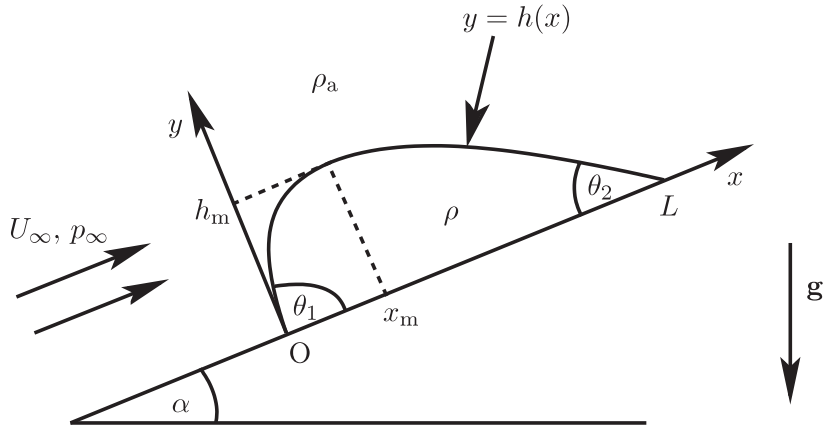

FIG. 1. Sketch of a steady thin sessile ridge of fluid on an inclined planar substrate in the presence of a steady inviscid airflow parallel to the substrate far from the ridge with constant speed U_∞ and ambient pressure p_∞.

analytical results for clarity. Note that, since the problem has two different length scales in the y direction, two different non-dimensional y-coordinates, namely y^* and Y^*, are required. The coordinate y^*, which corresponds to variation over the characteristic thickness scale for the ridge, ϵL_0 ($\ll L_0$) is required to describe the behaviour of the ridge; in particular, the internal pressure in the ridge, p^*, depends on x^* and y^*. On the other hand, the coordinate Y^*, which corresponds to variation over the characteristic length scale L_0, is required to describe the behaviour of the airflow; in particular, the external pressure in the air, P^*, depends on x^* and Y^*. For clarity we immediately drop the star superscripts on non-dimensional variables in what follows.

The airflow consists of a uniform stream with constant speed U_∞ in the positive x-direction plus a non-uniform perturbation due to the presence of the ridge, which we obtain to $O(\epsilon)$ using thin-aerofoil theory (see, for example, Van Dyke[44]). The velocity potential and stream function of the airflow $\phi(x,Y)$ and $\psi(x,Y)$ (both non-dimensionalised with L_0U_∞) are given in terms of the unknown free surface profile of the ridge by

$$\phi(x,Y) = x + \frac{\epsilon}{2\pi}\int_0^L h'(\xi)\,\log\left[(x-\xi)^2+Y^2\right]\,\mathrm{d}\xi, \tag{4}$$

$$\psi(x,Y) = Y + \frac{\epsilon}{\pi}\int_0^L h'(\xi)\tan^{-1}\left(\frac{Y}{x-\xi}\right)\,\mathrm{d}\xi, \tag{5}$$

satisfying $\psi(x,0) = 0$, where a prime denotes differentiation with respect to argument. Using either (4) or (5) together with Bernoulli's theorem yields an expression for the external pressure $P(x,Y)$, namely

$$P(x,Y) = -\Lambda\int_0^L \frac{(x-\xi)h'(\xi)}{(x-\xi)^2+Y^2}\,\mathrm{d}\xi, \tag{6}$$

where the non-dimensional Weber number, denoted by Λ and defined by

$$\Lambda = \frac{\rho_a L_0 U_\infty^2}{\pi\sigma}\,(\geq 0), \tag{7}$$

is the appropriate measure of the strength of the airflow (specifically, it represents the relative strengths of pressure forces and capillary forces).

Note that, since the airflow is inviscid, the sign of U_∞ is unimportant and hence the profile of the ridge will be the same whether the airflow is directed up or down the substrate. For definiteness we take the former, as indicated in Figure 1. Furthermore, since the airflow imposes a pressure gradient but no shear stress on the free surface of the ridge, there is no flow within the ridge. Of course, in reality the airflow will never be perfectly inviscid, and so there will always be some shear stress exerted on the free surface of the ridge and hence some flow within it. Specifically, a standard boundary-layer analysis shows that the shear stress exerted on the ridge is $O(\rho_a U_\infty^2\,\mathrm{Re}^{-1/2})$, where $\mathrm{Re} \gg 1$ is the local Reynolds number of the airflow. Hence, using, for example, the thin-film equation derived by King and Tuck [Ref. 26, Eq. (2.1)], the present analysis, which neglects effects due to surface shear stress relative to those due to the external pressure gradient, is appropriate when $\epsilon\rho_a U_\infty^2/L_0 \gg \rho_a U_\infty^2\,\mathrm{Re}^{-1/2}/(\epsilon L_0)$, i.e., when $\epsilon^4\,\mathrm{Re} \gg 1$.

In the absence of surface shear stress, the internal pressure $p(x,y)$ satisfies the hydrostatic equations

$$\epsilon p_x = -\left(\frac{L_0}{\ell}\right)^2\sin\alpha \qquad \text{and} \qquad p_y = -\left(\frac{L_0}{\ell}\right)^2\cos\alpha \tag{8}$$

subject to a balance of normal stress at the free surface $y = h$, namely $p = P - h''$ at $Y = 0$, where $\ell = (\sigma/\rho g)^{1/2}$ denotes the usual capillary length, in which g denotes the constant magnitude of gravitational acceleration. Integrating the second equation in (8) subject to the boundary condition gives

$$p = \left(\frac{L_0}{\ell}\right)^2(h-y)\cos\alpha + P - h''. \tag{9}$$

Substituting this solution for p into the first equation in (8) and evaluating the expression for P given by (6) at $Y = 0$ yields the governing linear singular integro-differential equation for h, namely

$$h''' - \left(\frac{L_0}{\ell}\right)^2 h' \cos\alpha - \left(\frac{L_0}{\ell}\right)^2 \frac{\sin\alpha}{\epsilon} + \Lambda \frac{\mathrm{d}}{\mathrm{d}x} \int_0^L \frac{h'(\xi)}{x-\xi}\,\mathrm{d}\xi = 0, \tag{10}$$

where the integral is of Cauchy principal-value type. Equation (10) is to be solved subject to boundary conditions of zero thickness at both contact lines and of prescribed constant volume, namely

$$h(0) = 0, \quad h(L) = 0, \quad V = \int_0^L h\,\mathrm{d}x. \tag{11}$$

Note that not all of the terms in (10) are necessarily of the same order in the thin-film limit $\epsilon \to 0$, and so, as described subsequently, the appropriate form of (10) depends on the particular physical situation under investigation.

III. A VERY WIDE SESSILE RIDGE

When the substrate is nearly horizontal (specifically, when $\alpha = O(\epsilon)$), the transverse component of gravity is relatively weak and so a very wide ridge of width comparable to the capillary length ℓ can be supported against gravity by capillary and/or external pressure forces. In this case it is appropriate to choose $L_0 = \ell$, so that $\epsilon = V/L_0^2 = V/\ell^2 \ll 1$, the characteristic pressure scale is $\epsilon\sigma/\ell = \epsilon\rho g\ell = \rho g V/\ell$, and at leading order in the limit $\epsilon \to 0$ Equation (10) becomes

$$h''' - h' - \hat{\alpha} + \Lambda \frac{\mathrm{d}}{\mathrm{d}x} \int_0^L \frac{h'(\xi)}{x-\xi}\,\mathrm{d}\xi = 0, \tag{12}$$

where

$$\Lambda = \frac{\rho_a \ell U_\infty^2}{\pi\sigma} \tag{13}$$

and the non-dimensional parameter $\hat{\alpha}$ (≥ 0), defined by

$$\hat{\alpha} = \frac{\alpha}{\epsilon}, \tag{14}$$

is an appropriately scaled version of the angle of inclination of the substrate to the horizontal. Equation (12) is subject to boundary conditions (11) and is analysed in detail below and in Secs. IV and V. The corresponding equations in the pendent case (specifically, when $\pi - \alpha = O(\epsilon)$) and in the case of a narrower (but still wide) sessile or pendent ridge (specifically, when $\alpha = O(1)$) are derived and analysed in Secs. VI and VII, respectively.

A. Local behaviour near the contact lines

Local analysis of (12) reveals that near the downslope and upslope contact lines, h behaves according to

$$h \sim \theta_1 x - \frac{\Lambda\theta_1}{2} x^2 \log x + \frac{\kappa_1}{2} x^2 \quad \text{as } x \to 0^+ \tag{15}$$

and

$$h \sim \theta_2 (L-x) - \frac{\Lambda\theta_2}{2} (L-x)^2 \log(L-x) + \frac{\kappa_2}{2} (L-x)^2 \quad \text{as } x \to L^-, \tag{16}$$

respectively, where the contact angles θ_1 and θ_2 and the constants κ_1 and κ_2 are determined globally (rather than locally). In particular, (15) and (16) show that h'' (but not h or h') is logarithmically singular at both contact lines for non-zero θ_1 and θ_2.

B. Transverse force balance

Multiplying Equation (12) by h, integrating with respect to x from 0 to L, and using the local behaviour (15) and (16) yields a statement of the transverse force balance on the ridge, namely

$$\theta_1^2 - \theta_2^2 - \Lambda \int_0^L \fint_0^L \frac{h'(x)h'(\xi)}{x-\xi}\,\mathrm{d}\xi\,\mathrm{d}x = 2V\hat{\alpha}. \tag{17}$$

A simple change of variables shows that the double integral in (17) is identically zero for regular (non-singular) $h'(x)$ in $0 \le x \le L$. Hence, since in the present problem, as in that studied by Durbin[25] but *not* in that studied by King and Tuck,[26] there are finite contact angles at both contact lines, Equation (17) reduces to simply

$$\theta_1^2 - \theta_2^2 = 2V\hat{\alpha}, \tag{18}$$

which is equivalent to Durbin's equation (A6).

The transverse force balance (18) shows immediately that $0 \le \theta_2 \le \theta_1$, i.e., that the ridge is always skewed in the downslope direction, with $\theta_1 = \theta_2$ only in the special case of a horizontal substrate, $\hat{\alpha} = 0$. Moreover, there is a critical ridge profile which occurs when $\theta_2 = 0$ (i.e., when the upslope contact angle reaches its minimum physically realisable value of zero). For a prescribed value of $\hat{\alpha}$, this critical profile occurs at a critical maximum Weber number Λ, denoted by $\Lambda = \Lambda_{\max}(\hat{\alpha})$, above which there are no physically realisable steady solutions and, conversely, for a prescribed value of Λ, it occurs at a critical maximum angle of inclination of the substrate $\hat{\alpha}$, denoted by $\hat{\alpha} = \hat{\alpha}_{\max}(\Lambda)$, above which there are again no physically realisable steady solutions. The critical quantities $\Lambda_{\max}$ and $\hat{\alpha}_{\max}$ will be discussed further in Secs. IV and V.

C. General form of the solution for the ridge profile

Inspection of (11) and (12) reveals that the general form of the solution for $h = h(x)$ is a linear function of V and $\hat{\alpha}$, namely $h = Vh_0 + \hat{\alpha}h_1$, with

$$h_0(0) = h_0(L) = h_1(0) = h_1(L) = 0, \quad \int_0^L h_0\,\mathrm{d}x = 1, \quad \int_0^L h_1\,\mathrm{d}x = 0, \tag{19}$$

where the function $h_0 = h_0(x)$, which represents the ridge profile in the special case $\hat{\alpha} = 0$, is positive and symmetric about $x = L/2$, and the function $h_1 = h_1(x)$ is antisymmetric about $x = L/2$. In general, we must solve (12) subject to (11) for h numerically, and we do this using a finite difference method, the details of which are given by Paterson.[45] Figure 2 shows numerically calculated plots of h_0 and h_1 when $L = 1$ for various values of Λ satisfying $\Lambda \le \Lambda_{\max}(0) \simeq 2.25$. Since h_1 is positive for $0 < x < L/2$ and negative for $L/2 < x < L$, Figure 2 shows that, in accordance with (18), increasing $\hat{\alpha}$ (i.e., tilting the substrate) always skews the ridge downslope, so that h_{m} increases, x_{m} decreases (i.e., moves downslope), θ_1 increases, and θ_2 decreases.

IV. STRENGTHENING THE EXTERNAL AIRFLOW

In this section we investigate the quasi-static evolution of a very wide sessile ridge on a substrate inclined at a constant angle $\hat{\alpha}$ to the horizontal as the airflow is gradually strengthened (i.e., as Λ is gradually increased from zero). In Sec. IV A we consider a pinned ridge (i.e., a ridge with pinned contact lines), and hence constant width L but variable contact angles θ_1 and θ_2. In reality, the contact lines will not remain pinned for all values of $\Lambda \le \Lambda_{\max}$ (i.e., for all values of $\theta_2 \ge 0$). In practice (as, for example, Dussan[46] and Blake and Ruschak[47] describe), eventually one or both of θ_1 and θ_2 will reach either the receding contact angle, θ_{R}, or the advancing contact angle, θ_{A}, and the corresponding contact line(s) will de-pin. For definiteness, we assume that θ_1 and θ_2 satisfy $\theta_{\mathrm{R}} \le \theta_{1,2} \le \theta_{\mathrm{A}}$ when $\Lambda = 0$, i.e., that the ridge is always pinned in the absence of the airflow. We will find that increasing the strength of the airflow Λ decreases θ_1 and θ_2, and so, while neither θ_1 nor θ_2 can ever reach θ_{A}, they may reach θ_{R}. However, as previously noted, Equation (18) shows that $\theta_2 \le \theta_1$, and so (except in the special case $\hat{\alpha} = 0$ in which $\theta_1 = \theta_2$), θ_2 will always reach θ_{R} before θ_1 does (i.e., the upslope contact

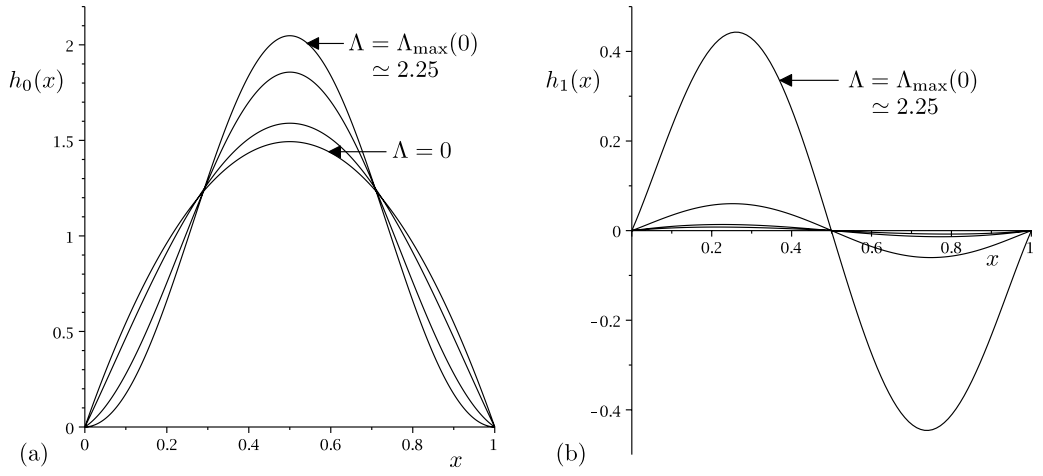

FIG. 2. Plots of the functions (a) $h_0(x)$ and (b) $h_1(x)$ appearing in the general form of the solution for the ridge profile, $h = Vh_0 + \hat{\alpha}h_1$, for $\Lambda = 0$, 1, 2, $\Lambda_{\max}(0) \simeq 2.25$ when $L = 1$.

line will always de-pin before the downslope one). After de-pinning we assume that θ_2 remains equal to θ_R, and hence from (18) that $\theta_1 = (\theta_R^2 + 2V\hat{\alpha})^{1/2}$ ($\geq \theta_R$). Thus in Sec. IV B we consider a ridge that de-pins at its upslope contact line, and hence after de-pinning has variable width L but constant contact angles $\theta_1 = (\theta_R^2 + 2V\hat{\alpha})^{1/2}$ and $\theta_2 = \theta_R$.

A. A pinned ridge

1. The limit of a weak external airflow ($\Lambda \to 0^+$)

In the limit of a weak airflow, $\Lambda \to 0^+$, the ridge profile takes the form $h = H_0 + \Lambda H_1 + O(\Lambda^2)$.

The leading order term, $H_0 = H_0(x)$, is simply the profile in the special case of no airflow, $\Lambda = 0$, which can be obtained from the solution given by Diez *et al.* [Ref. 48, Eq. (5)] and is given by $H_0 = Vh_0 + \hat{\alpha}h_1$, where the functions $h_0 = h_0(x)$ and $h_1 = h_1(x)$ are given by

$$h_0 = \frac{\sinh\frac{L-x}{2}\sinh\frac{x}{2}}{\frac{L}{2}\cosh\frac{L}{2} - \sinh\frac{L}{2}} \quad \text{and} \quad h_1 = \frac{L\cosh\frac{L-x}{2}\sinh\frac{x}{2}}{\sinh\frac{L}{2}} - x, \tag{20}$$

respectively. Using (20) it may readily be deduced that θ_1 and θ_2 are given by

$$\theta_{1,2} = V\gamma \pm \frac{\hat{\alpha}}{2\gamma}, \tag{21}$$

where the + sign is taken for θ_1, the − sign is taken for θ_2, and the function $\gamma = \gamma(L)$ (> 0) is defined by

$$\gamma = \frac{1}{2}\left(\frac{L}{2}\coth\frac{L}{2} - 1\right)^{-1}. \tag{22}$$

Inspection of (22) reveals that γ is a strictly positive, monotonically decreasing function of L and satisfies $\gamma \sim 6/L^2 \to \infty$ as $L \to 0^+$ and $\gamma \sim 1/L \to 0^+$ as $L \to \infty$. Hence, from (21) it can be deduced that as L is increased both contact angles decrease, with θ_2 reaching zero and θ_1 reaching the non-zero value $\theta_1 = 2V\gamma = \hat{\alpha}/\gamma$ when $\hat{\alpha} = 2V\gamma^2$, and hence the critical maximum value of $\hat{\alpha}$ when $\Lambda = 0$ is given by $\hat{\alpha}_{\max}(0) = 2V\gamma^2$. Figure 3(a) shows plots of H_0 for various values of $\hat{\alpha}$ when $L = 1$, in which case $\hat{\alpha}_{\max}(0) \simeq 74.40$. In particular, Figure 3(a) shows that, as previously noted, tilting the substrate skews the ridge downslope.

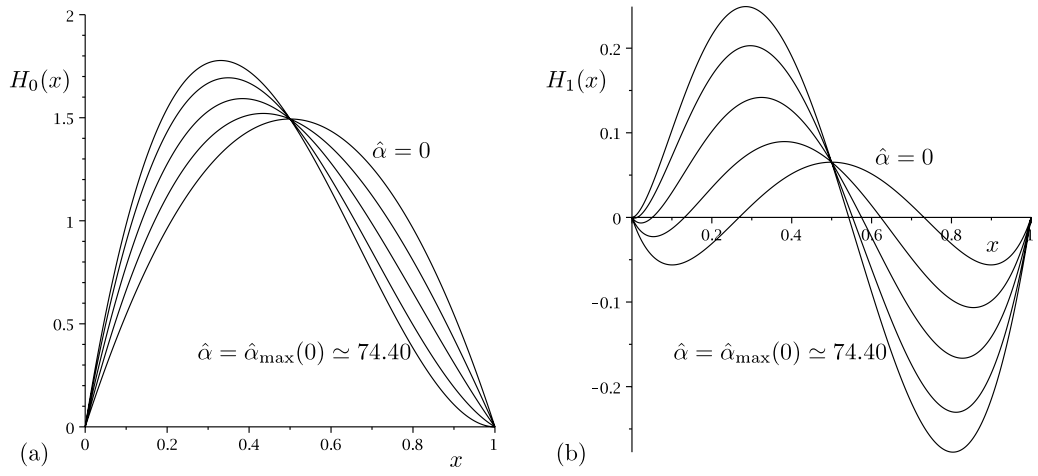

FIG. 3. Plots of (a) the leading order term, $H_0(x)$, and (b) the first order term, $H_1(x)$, in the asymptotic solution for the profile of a pinned ridge in the limit of a weak airflow, $\Lambda \to 0^+$, given by $h = H_0 + \Lambda H_1 + O(\Lambda^2)$ for $\hat{\alpha} = 0, 20, 40, 60, \hat{\alpha}_{\max}(0) \simeq 74.40$ when $L = 1$.

The first order term, $H_1 = H_1(x)$, satisfies

$$H_1''' - H_1' + \frac{\mathrm{d}}{\mathrm{d}x}\int_0^L \frac{H_0'(\xi)}{x-\xi}\,\mathrm{d}\xi = 0 \tag{23}$$

subject to

$$H_1(0) = 0, \quad H_1(L) = 0, \quad \int_0^L H_1\,\mathrm{d}x = 0. \tag{24}$$

Figure 3(b) shows numerically calculated plots of H_1 for various values of $\hat{\alpha}$ when $L = 1$. In the special case of a horizontal substrate, $\hat{\alpha} = 0$, H_1 is symmetric about $x = L/2$ with $H_1 > 0$ and $H_1' = 0$ at $x = x_{\mathrm{m}} = L/2$, and $-H_1'(L) = H_1'(0) < 0$. Therefore, in this case the effect of a weak airflow is to slightly decrease both contact angles equally, and to slightly increase h_{m} (which always occurs at $x = x_{\mathrm{m}} = L/2$), i.e., to push the ridge down near to its edges and pull it up near to its middle. In the general case of a tilted substrate, $0 < \hat{\alpha} \le \hat{\alpha}_{\max}$, H_1 is no longer symmetric about $x = L/2$, with $x = x_{\mathrm{m}}$ satisfying $0 < x_{\mathrm{m}} < L/2$, and $-H_1'(L) < H_1'(0) \le 0$ with $H_1'(0) = 0$ at $\hat{\alpha} = \hat{\alpha}_{\max}(0)$. Therefore, in this case the effect of a weak airflow is to slightly decrease both contact angles (but to decrease θ_2 more than θ_1), and to slightly increase h_{m} and to slightly decrease x_{m}, i.e., to skew the ridge downslope while simultaneously pushing it down near to its edges and pulling it up near to its middle.

2. The general case of non-zero external airflow ($\Lambda > 0$)

Figure 4(a) shows plots of the profile of a pinned ridge as Λ is increased from $\Lambda = 0$ to $\Lambda = \Lambda_{\max} \simeq 1.50$ when $\hat{\alpha} = 20$ and $L = 1$. Figures 4(b)–4(d) show how θ_1 and θ_2, h_{m}, and x_{m}/L vary with Λ for a range of values of $\hat{\alpha}$. In particular, Figure 4(b) shows that both θ_1 and θ_2 decrease monotonically with Λ, and that $\mathrm{d}\theta_1/\mathrm{d}\Lambda = 0$ when $\theta_2 = 0$ (i.e., at $\Lambda = \Lambda_{\max}$). Furthermore, Figures 4(c) and 4(d) show that h_{m} increases monotonically and x_{m}/L decreases monotonically with Λ (except in the special case $\hat{\alpha} = 0$, in which the ridge is symmetric about $x = x_{\mathrm{m}} = L/2$ for all Λ).

Figure 5 shows the relationship between $\hat{\alpha}_{\max}$ and $\Lambda_{\max}$ (i.e., between the critical values of $\hat{\alpha}$ and Λ and for which $\theta_2 = 0$) for various values of L. This plot may be interpreted as giving either $\Lambda_{\max}$ as a function of $\hat{\alpha}$ or $\hat{\alpha}_{\max}$ as a function of Λ. Figure 5 shows that, for a given value of L, the largest possible value of $\hat{\alpha}_{\max}$ occurs at $\Lambda = 0$ (i.e., is equal to $\hat{\alpha}_{\max}(0)$), and the largest possible value of $\Lambda_{\max}$ occurs at $\hat{\alpha} = 0$ (i.e., is equal to $\Lambda_{\max}(0)$). For example, in Figures 4(b)–4(d) the largest possible value of Λ is $\Lambda_{\max}(0) \simeq 2.25$, and the largest possible value of $\hat{\alpha}$ is $\hat{\alpha}_{\max}(0) \simeq 74.40$.

The results shown in Figure 4 confirm the behaviour evident in the limit of a weak airflow described in Sec. IV A 1, namely that the effect of strengthening the airflow is to skew the ridge

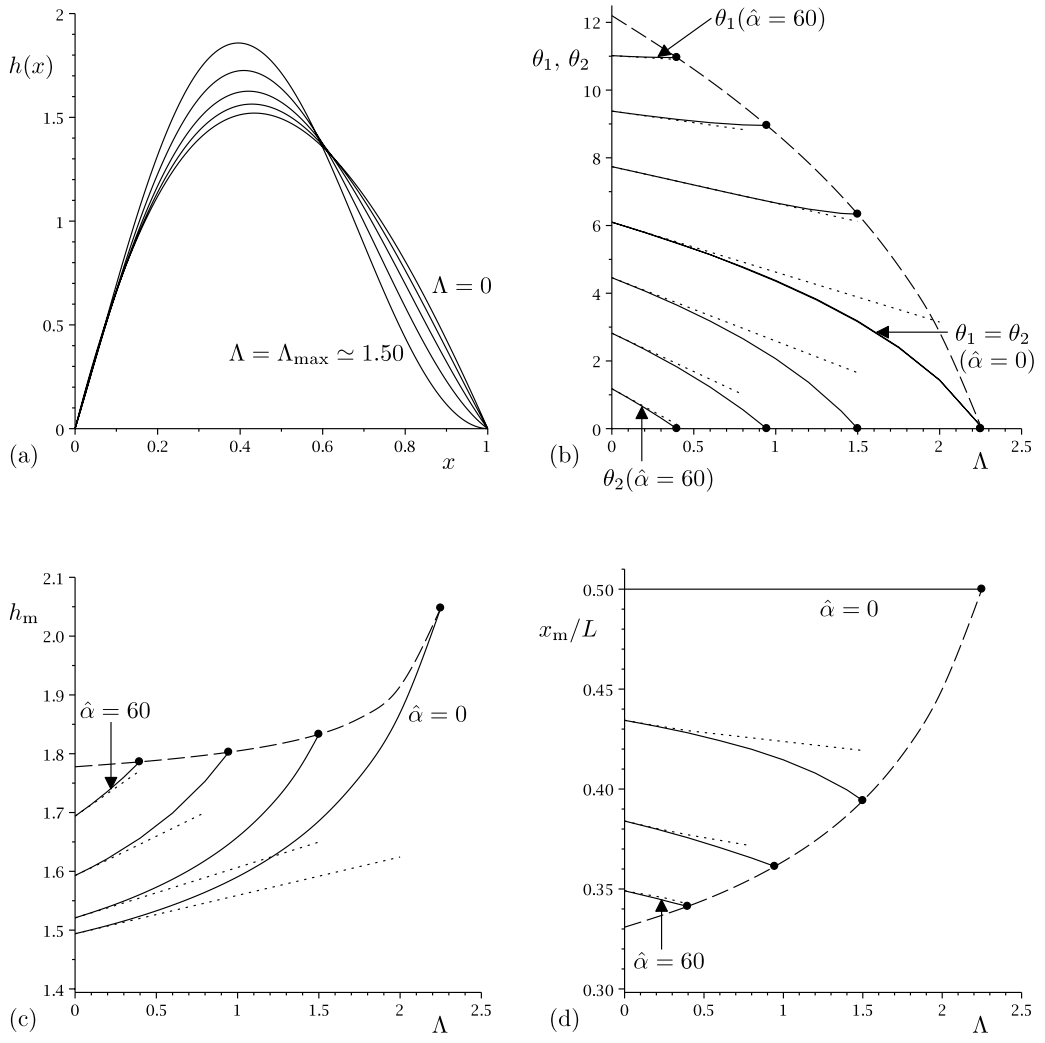

FIG. 4. Plots of (a) the profile of a very wide sessile pinned ridge for $\Lambda = 0$, 0.4, 0.8, 1.2, $\Lambda_{\max} \simeq 1.50$ when $\hat{\alpha} = 20$ and $L = 1$, together with plots of (b) the contact angles θ_1 and θ_2, (c) the maximum thickness h_{m}, and (d) the relative location of the maximum thickness x_{m}/L, as functions of Λ for a very wide sessile pinned ridge for $\hat{\alpha} = 0$, 20, 40, 60 when $L = 1$ (in which case $\Lambda_{\max}(0) \simeq 2.25$ and $\hat{\alpha}_{\max}(0) \simeq 74.40$). In (b)–(d) the dots indicate the points at which $\theta_2 = 0$ (i.e., when $\Lambda = \Lambda_{\max}$), the dashed lines show the curves on which $\Lambda = \Lambda_{\max}$, and the dotted lines show the first-order-accurate asymptotic solutions in the limit of a weak airflow, $\Lambda \to 0^+$.

downslope while simultaneously pushing it down near to its edges and pulling it up near to its middle. In order to understand why the airflow has this effect on the ridge, it is instructive to investigate the external pressure due to the airflow given by (6) in more detail.

Figure 6(a) shows $P(x,0)$ plotted as a function of x for various values of Λ when $\hat{\alpha} = 20$ and $L = 1$ (i.e., for the pinned ridge whose profile is shown in Figure 4(a)). Figure 6(a) shows that the external pressure near $x = x_{\mathrm{m}}$ is lower than the ambient pressure far from the ridge, and that the external pressure near the downslope (leading) and upslope (trailing) edges of the ridge is higher than the ambient pressure. Using the local behaviour (15) and (16) shows that near the downslope contact line P behaves according to

$$P(x,0) \sim -\Lambda\theta_1 \log x \to \infty \quad \text{as } x \to 0^+ \tag{25}$$

for $\theta_1 > 0$, while near the upslope contact line P behaves according to

$$P(x,0) \sim -\Lambda\theta_2 \log(L - x) \to \infty \quad \text{as } x \to L^- \tag{26}$$

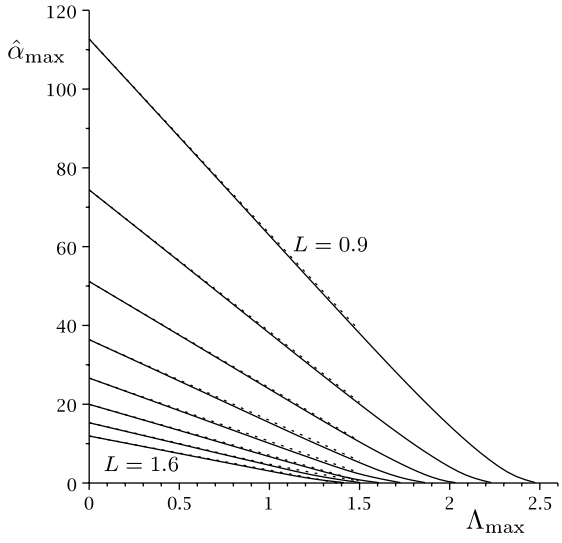

FIG. 5. Plot of the relationship between the critical inclination angle $\hat{\alpha}_{\max}$ and the critical Weber number $\Lambda_{\max}$ for $L = 0.9$, 1, 1.1, 1.2, 1.3, 1.4, 1.5, 1.6. The dotted lines show the first-order-accurate asymptotic solutions in the limit of a weak airflow, $\Lambda \to 0^+$.

for $\theta_2 > 0$ and

$$P(x,0) \sim \Lambda_{\max}\kappa_2 L = O(1) \quad \text{as } x \to L^- \tag{27}$$

for $\theta_2 = 0$, i.e., a non-zero contact angle leads to a logarithmic singularity in $P(x,0)$ at the corresponding contact line. Figure 6(b) shows $P(x,Y)$ plotted as a function of Y for various values of x in the range $-0.3 \le x/L \le x_m/L \simeq 0.41$ when $\Lambda = 1$, $\hat{\alpha} = 20$, and $L = 1$. Figure 6(b) shows that $P(x_m,Y)$ is negative at $Y = 0$ and increases monotonically towards zero as Y increases. Figure 6(b) also shows that $P(0,Y)$ is large and positive near $Y = 0$ and decreases towards zero as Y increases. $P(L,Y)$ has qualitatively the same behaviour as $P(0,Y)$, but for clarity values of x/L greater than $x_m/L \simeq 0.41$ are not shown in Figure 6(b). Figure 6(c) shows the streamlines of the airflow passing over the ridge plotted using (5) when $\Lambda = 1$, $\hat{\alpha} = 20$, $L = 1$, and $\epsilon = 0.05$. Far upstream and downstream of the ridge the flow is uniform and so the streamlines are parallel to the substrate, while near $x = x_m$ the curvature of the streamlines is (slightly) negative and so, given that the pressure increases in the direction away from the centre of curvature, the pressure there is (slightly) smaller than that of the uniform stream. Hence, the free surface tends to be pulled up near $x = x_m$ (i.e., h_m increases). Similarly, near the contact lines the streamline curvature is (slightly) positive and so the pressure near the contact lines is (slightly) larger than that of the uniform stream. Hence, the free surface tends to be pushed down near the contact lines (i.e., both θ_1 and θ_2 decrease).

B. A ridge that de-pins at its upslope contact line

As the strength of the airflow is increased from zero the ridge initially deforms but remains pinned with constant width as described in Sec. IV A. However, since both θ_1 and θ_2 ($\le\theta_1$) are monotonically decreasing functions of Λ, eventually at a critical airflow strength denoted by $\Lambda = \Lambda_R$ and satisfying $\Lambda_R \le \Lambda_{\max}$, the upslope contact angle θ_2 becomes equal to the receding contact angle θ_R and the upslope contact line de-pins. As the strength of the airflow is increased from $\Lambda = \Lambda_R$ the ridge continues to deform but now with varying width L. Figure 7(a) shows plots of the profile of a de-pinned ridge as Λ is increased from $\Lambda = \Lambda_R \simeq 1.02$ when $\hat{\alpha} = 20$ and $\theta_R = 2$. Note that for clarity the corresponding pinned ridge profiles for $0 \le \Lambda < \Lambda_R$ are not shown in Figure 7(a), but examples have, of course, already been shown in Figure 4(a). Figures 7(b)–7(e) show how θ_1 and θ_2, h_m, x_m/L, and L vary with Λ for a range of values of $\hat{\alpha}$ when $\theta_R = 2$. Note that for $\Lambda < \Lambda_R$ (i.e., to the left of the dots denoting the points at which the upslope contact line de-pins), the curves in Figures 7(b)–7(d) are identical

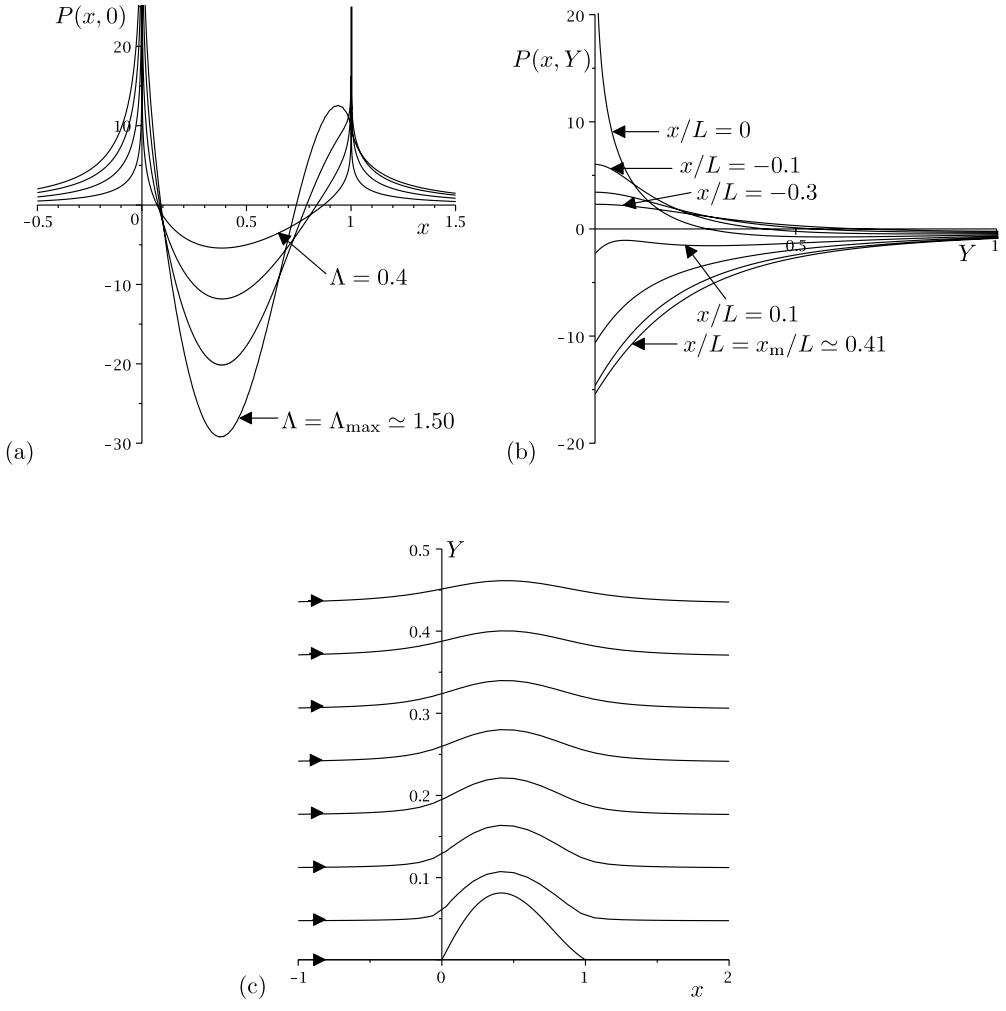

FIG. 6. Plots of (a) the external pressure at the free surface of the ridge and the substrate, $P(x,0)$, as a function of x for $\Lambda = 0, 0.4, 0.8, 1.2, \Lambda_{\max} \simeq 1.50$ when $\hat{\alpha} = 20$ and $L = 1$, (b) the external pressure, $P(x,Y)$, as a function of Y at $x/L = -0.3$, -0.2, -0.1, 0, 0.1, 0.2, 0.3, $x_m/L \simeq 0.41$ when $\Lambda = 1$, $\hat{\alpha} = 20$, and $L = 1$, and (c) the streamlines of the airflow passing over the ridge when $\Lambda = 1$, $\hat{\alpha} = 20$, $L = 1$, and $\epsilon = 0.05$.

to the corresponding curves for a pinned ridge shown in Figures 4(b)–4(d). Figure 7(b) shows that after the contact line has de-pinned (i.e., for $\Lambda > \Lambda_R$) $\theta_1 = (\theta_R^2 + 2V\hat{\alpha})^{1/2}$ and $\theta_2 = \theta_R$ are independent of the value of Λ. Moreover, Figures 7(c)–7(e) show that while h_m and L are monotonically increasing and decreasing functions of Λ, respectively, x_m/L decreases to a minimum value at $\Lambda = \Lambda_R$ before increasing towards the limiting value of $x_m/L = 1/2$ as Λ becomes large.

In the limit of a strong airflow, $\Lambda \to \infty$, the numerically calculated solutions shown in Figure 7 suggest that the ridge becomes narrow like $L = O(\Lambda^{-1}) \to 0^+$ and thick like $h_m = O(\Lambda) \to \infty$ with $x_m/L \to 1/2^-$. To investigate the behaviour of the ridge in this limit we therefore rescale the variables according to

$$L = \Lambda^{-1}\bar{L}, \quad x = \Lambda^{-1}\bar{L}\bar{x}, \quad x_m = \Lambda^{-1}\bar{L}\bar{x}_m, \quad \xi = \Lambda^{-1}\bar{L}\bar{\xi}, \quad h = \Lambda\bar{L}^{-1}\bar{h}, \quad h_m = \Lambda\bar{L}^{-1}\bar{h}_m, \quad (28)$$

where the leading order scaled width $\bar{L}$ is to be determined as part of the solution. At leading order in the limit $\Lambda \to \infty$ the effect of gravity is negligible, and (12) and (11) become

$$\bar{h}''' + \bar{L}\frac{\mathrm{d}}{\mathrm{d}\bar{x}}\int_0^1 \frac{\bar{h}'(\bar{\xi})}{\bar{x} - \bar{\xi}}\,\mathrm{d}\bar{\xi} = 0 \quad (29)$$

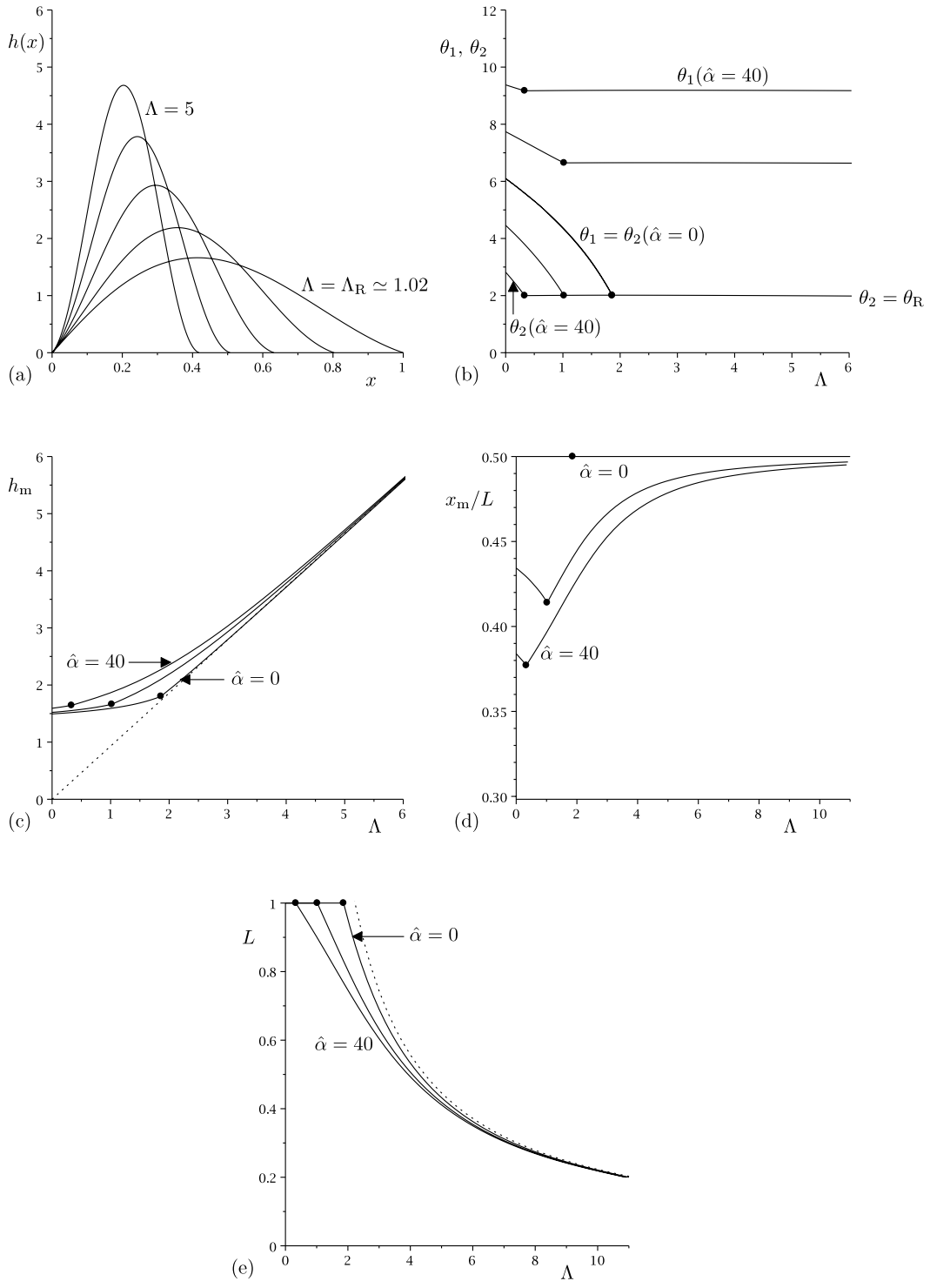

FIG. 7. Plots of (a) the profile of a very wide sessile de-pinned ridge for $\Lambda = \Lambda_R \simeq 1.02$, 2, 3, 4, 5 when $\hat{\alpha} = 20$ and $\theta_R = 2$, together with plots of (b) the contact angles θ_1 and θ_2, (c) the maximum thickness h_m, (d) the relative location of the maximum thickness x_m/L, and (e) the width L, as functions of Λ for a very wide sessile ridge whose upslope contact line de-pins for $\hat{\alpha} = 0$, 20, 40 when $\theta_R = 2$ (in which case $\hat{\alpha}_{max}(0) \simeq 50.01$). In (b)–(e) the dots indicate the points at which the upslope contact line de-pins (i.e., when $\Lambda = \Lambda_R$ and $\theta_2 = \theta_R$), and in (c)–(e) the dotted lines show the leading order asymptotic solutions in the limit of a strong airflow, $\Lambda \to \infty$, given by (c) $h_m \simeq 0.94\Lambda \to \infty$, (d) $x_m/L = 1/2$ (which coincides with the solution in the special case $\hat{\alpha} = 0$), and (e) $L \simeq 2.20\Lambda^{-1} \to 0^+$ for all $\hat{\alpha}$.

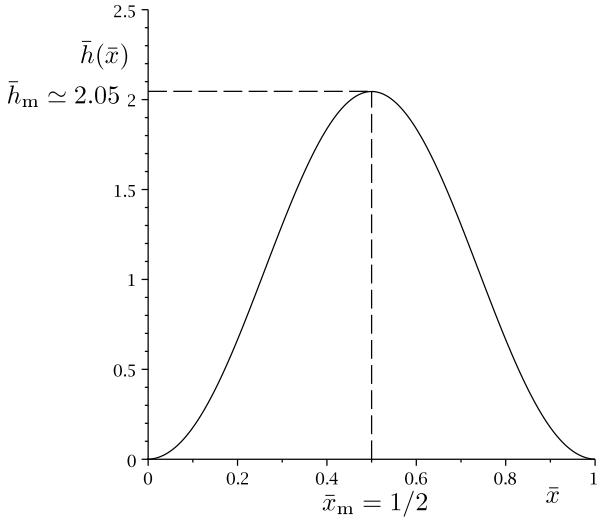

FIG. 8. Plot of the leading order scaled ridge profile $\bar{h}(\bar{x})$ in the limit of a strong airflow, $\Lambda \to \infty$, obtained by solving (29) subject to (30) numerically.

subject to

$$\bar{h}(0) = 0, \quad \bar{h}(1) = 0, \quad \bar{h}'(1) = 0, \quad \int_0^1 \bar{h}\,\mathrm{d}\bar{x} = V. \tag{30}$$

Equation (29) was solved subject to (30) numerically to obtain the solution for the leading order scaled ridge profile $\bar{h} = \bar{h}(\bar{x})$, and the leading order values $\bar{L} \simeq 2.20$, $\bar{h}_{\rm m} \simeq 2.05$, and $\bar{x}_{\rm m} = 1/2$. Figure 8 shows a plot of $\bar{h}(\bar{x})$, and shows that it is symmetric about $\bar{x} = \bar{x}_{\rm m} = 1/2$. The leading order asymptotic solutions for $h_{\rm m} \simeq 0.94\Lambda \to \infty$ and $L \simeq 2.20\Lambda^{-1} \to 0^+$ are shown with dotted lines in Figures 7(c) and 7(e), while in Figure 7(d) the leading order asymptotic solution for $x_{\rm m}/L = 1/2$ coincides with the solution in the special case $\hat{\alpha} = 0$. This asymptotic solution shows how the ridge becomes narrower, thicker, and closer to being symmetric in the limit of a strong airflow. The (scaled) aspect ratio of the ridge in this limit is $O(\Lambda^2) \gg 1$, and so while the underlying thin-film approximation will eventually fail when Λ becomes too large, the present asymptotic solution is useful provided that $V \ll \Lambda^2 V \ll \ell^2$.

V. TILTING THE SUBSTRATE

In this section we investigate the quasi-static evolution of a very wide sessile ridge in the presence of an airflow of constant strength Λ as the substrate is gradually tilted (i.e., as the angle of inclination of the substrate $\hat{\alpha}$ to the horizontal is gradually increased from zero). Like in Sec. IV A, in Sec. V A, we again consider a pinned ridge, and hence constant width L but variable contact angles θ_1 and θ_2. However, unlike in Sec. IV A, in which we found that increasing Λ decreases both θ_1 and θ_2, we will find that increasing $\hat{\alpha}$ increases θ_1 and decreases θ_2. Moreover, as the general form of the solution for the ridge profile shows, both θ_1 and θ_2 vary linearly with $\hat{\alpha}$. Like in Sec. IV, in reality the contact lines will not remain pinned for all values of $\hat{\alpha} \le \hat{\alpha}_{\rm max}$ (i.e., for all values of $\theta_2 \ge 0$). In practice, either θ_1 will reach $\theta_{\rm A}$ or θ_2 will reach $\theta_{\rm R}$ and the corresponding contact line(s) will de-pin. For definiteness we assume that θ_1 and θ_2 satisfy $\theta_{\rm R} \le \theta_{1,2} \le \theta_{\rm A}$ when $\hat{\alpha} = 0$, i.e., that the ridge is always pinned when the substrate is horizontal. However, unlike in Sec. IV, in which, in general, θ_2 always reaches $\theta_{\rm R}$ first as Λ is increased, now it is possible *either* for θ_2 to reach $\theta_{\rm R}$ first *or* for θ_1 to reach $\theta_{\rm A}$ first as $\hat{\alpha}$ is increased. After de-pinning we assume that either θ_2 remains equal to $\theta_{\rm R}$ and hence from (18) that $\theta_1 = (\theta_{\rm R}^2 + 2V\hat{\alpha})^{1/2}$ $(\ge\theta_{\rm R})$ is an increasing function of $\hat{\alpha}$, or θ_1 remains equal to $\theta_{\rm A}$ and hence from (18) that $\theta_2 = (\theta_{\rm A}^2 - 2V\hat{\alpha})^{1/2}$ $(\le\theta_{\rm A})$ is a decreasing function of $\hat{\alpha}$, as appropriate. In Sec. V B we consider the general situation in which both contact lines eventually de-pin, while in Secs. V C and V D we consider the special cases in which only the downslope contact line de-pins and only the upslope contact line de-pins, respectively.

A. A pinned ridge

Figure 9(a) shows plots of the profile of a pinned ridge as $\hat{\alpha}$ is increased from $\hat{\alpha} = 0$ to $\hat{\alpha}_{\max} \simeq 38.02$ when $\Lambda = 1$ and $L = 1$. Figures 9(b)–9(d) show how θ_1, θ_2, h_m, and x_m/L vary with $\hat{\alpha}$ for a range of values of Λ. In particular, Figure 9(b) shows that θ_1 increases linearly and θ_2 decreases linearly with $\hat{\alpha}$. Furthermore, Figures 9(c) and 9(d) show that h_m increases monotonically and x_m/L decreases monotonically with $\hat{\alpha}$. Note that, as in Figures 4(b)–4(d) discussed previously in Sec. IV A, in Figures 9(b)–9(d) (which correspond to the same values of L and V) the largest possible value of Λ is $\Lambda_{\max}(0) \simeq 2.25$, and the largest possible value of $\hat{\alpha}$ is $\hat{\alpha}_{\max}(0) \simeq 74.40$.

B. A ridge that eventually de-pins at both of its contact lines

In the general case in which θ_A is finite and θ_R is non-zero, the ridge eventually de-pins at both of its contact lines for increasing $\hat{\alpha}$, but the order in which the contact lines de-pin depends on the value of Λ. Specifically, if θ_1 reaches θ_A at some value $\hat{\alpha} = \hat{\alpha}_A(\Lambda)$ ($< \hat{\alpha}_{\max}(\Lambda)$), before θ_2 reaches

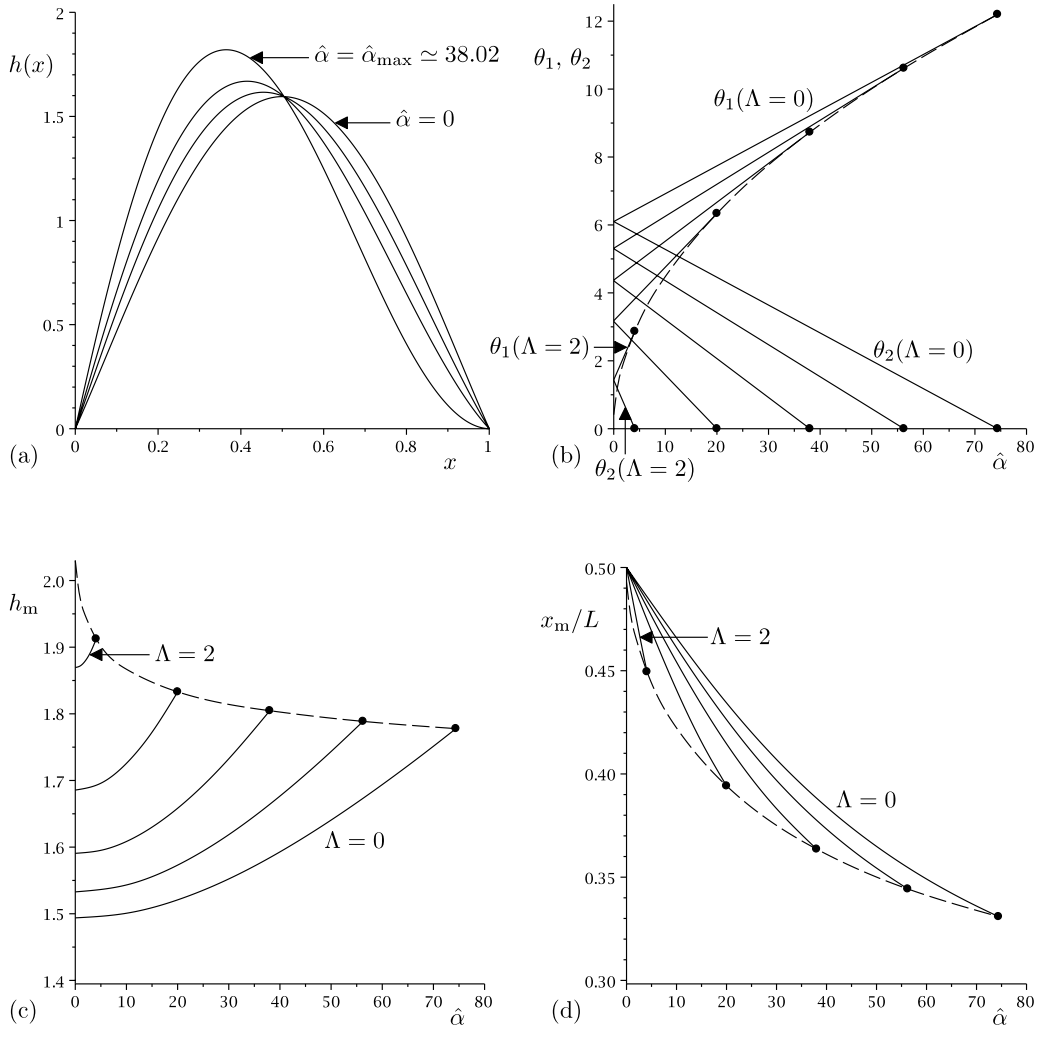

FIG. 9. Plots of (a) the profile of a very wide sessile pinned ridge for $\hat{\alpha} = 0$, 10, 20, $\hat{\alpha}_{\max} \simeq 38.02$ when $\Lambda = 1$ and $L = 1$, together with plots of (b) the contact angles θ_1 and θ_2, (c) the maximum thickness h_m, and (d) the relative location of the maximum thickness x_m/L, as functions of $\hat{\alpha}$ for a very wide sessile pinned ridge for $\Lambda = 0$, 0.5, 1, 1.5, and 2 when $L = 1$ (in which case $\Lambda_{\max}(0) \simeq 2.25$ and $\hat{\alpha}_{\max}(0) \simeq 74.40$). In (b)–(d) the dots indicate the points at which $\theta_2 = 0$ (i.e., when $\hat{\alpha} = \hat{\alpha}_{\max}$) and the dashed lines show the curves on which $\hat{\alpha} = \hat{\alpha}_{\max}$.

θ_R, then the downslope contact line will de-pin first, but if θ_2 reaches θ_R at some value $\hat{\alpha} = \hat{\alpha}_R(\Lambda)$ ($< \hat{\alpha}_{max}(\Lambda)$), before θ_1 reaches θ_A, then the upslope contact line will de-pin first. Regardless of which contact line de-pins first, the second contact line de-pins when *both* $\theta_1 = \theta_A$ *and* $\theta_2 = \theta_R$, and hence from (18) this always occurs at $\hat{\alpha} = \hat{\alpha}_{AR}$, where

$$\hat{\alpha}_{AR} = \frac{\theta_A^2 - \theta_R^2}{2V}, \tag{31}$$

which is independent of the value of Λ, and for $\hat{\alpha} > \hat{\alpha}_{AR}$ there are no steady solutions of the kind considered here. There is a critical value of Λ, denoted by Λ_{AR}, for which the two contact lines de-pin simultaneously (i.e., $\theta_1 = \theta_A$ and $\theta_2 = \theta_R$ simultaneously for the first time at $\hat{\alpha} = \hat{\alpha}_{AR}$). The value of Λ relative to Λ_{AR} determines which of the two contact lines de-pins first for increasing $\hat{\alpha}$: if $\Lambda < \Lambda_{AR}$ then the downslope contact line de-pins first, while if $\Lambda > \Lambda_{AR}$ then the upslope contact line de-pins first.

Figures 10(a) and 10(b) show plots of the profile of a ridge as $\hat{\alpha}$ is increased from $\hat{\alpha} = 0$ to $\hat{\alpha} = \hat{\alpha}_{AR} = 45/2 = 22.50$ in the cases $\Lambda < \Lambda_{AR} \simeq 0.93$ and $\Lambda > \Lambda_{AR}$, respectively, when $\theta_A = 7$ and $\theta_R = 2$. Figures 10(c)–10(f) show how θ_1 and θ_2, h_m, x_m/L, and L vary with $\hat{\alpha}$ for a range of values of Λ when $\theta_A = 7$ and $\theta_R = 2$. Note that until the first contact line de-pins (i.e., to the left of the leftmost dots denoting the points at which the first contact line de-pins), the curves in Figures 10(c)–10(e) are identical to the corresponding curves for a pinned ridge shown in Figures 9(b)–9(d). In particular, Figures 10(c) and 10(f) show that if $\Lambda < \Lambda_{AR}$ then the downslope contact line de-pins first and the width of the ridge increases after de-pinning, if $\Lambda > \Lambda_{AR}$ then the upslope contact line de-pins first and the width of the ridge decreases after de-pinning, and if $\Lambda = \Lambda_{AR}$ then the two contact lines de-pin simultaneously.

C. A ridge that de-pins only at its downslope contact line

In the special case $\theta_R = 0$ the upslope contact line remains pinned for all values of $\theta_2 \geq 0$, while the downslope contact line de-pins at $\hat{\alpha} = \hat{\alpha}_A$. Figure 11(a) shows plots of the profile of a ridge that has de-pinned at its downslope contact line as $\hat{\alpha}$ is increased from $\hat{\alpha} = \hat{\alpha}_A \simeq 23.08$ to $\hat{\alpha} = \hat{\alpha}_{Amax} = 49/2 = 24.50$ when $\Lambda = 1$, $\theta_A = 7$, and $\theta_R = 0$. Figures 11(b)–11(e) show how θ_1 and θ_2, h_m, x_m/L, and L vary with $\hat{\alpha}$ for a range of values of Λ when $\theta_A = 7$ and $\theta_R = 0$. In particular, Figure 11(e) shows that the width of the ridge always increases after de-pinning. The upslope contact angle eventually reaches the value $\theta_2 = \theta_R = 0$ when $\theta_A^2 = 2V\hat{\alpha}$, and so, as Figures 11(b)–11(e) show, there is a maximum value of $\hat{\alpha} = \hat{\alpha}_{Amax} = \theta_A^2/2V$ ($= \hat{\alpha}_{AR}$ evaluated at $\theta_R = 0$), which is independent of the value of Λ, at which the ridge achieves its maximum width and beyond which there are no steady solutions of the kind considered here.

D. A ridge that de-pins only at its upslope contact line

In the special case $\theta_A = \infty$ the downslope contact line remains pinned for all values of θ_1, while the upslope contact line de-pins at $\hat{\alpha} = \hat{\alpha}_R$. Figure 12(a) shows plots of the profile of a ridge that has de-pinned at its upslope contact line as $\hat{\alpha}$ is increased from $\hat{\alpha} = \hat{\alpha}_R \simeq 20.58$ when $\Lambda = 1$, $\theta_A = \infty$, and $\theta_R = 2$. Figures 12(b)–12(e) show how θ_1 and θ_2, h_m, x_m/L, and L vary with $\hat{\alpha}$ for a range of values of Λ when $\theta_A = \infty$ and $\theta_R = 2$. In particular, Figure 12(e) shows that the width of the ridge always decreases after de-pinning.

In the limit of a large angle of inclination of the substrate, $\hat{\alpha} \to \infty$, the numerically calculated solutions shown in Figure 12 suggest that the ridge becomes narrow like $L = O(\hat{\alpha}^{-1/4}) \to 0^+$ and thick like $h_m = O(\hat{\alpha}^{1/4}) \to \infty$ with $x_m/L \to 1/3^+$. To investigate the behaviour of the ridge in this limit we therefore rescale the variables according to

$$\begin{gathered} L = \hat{\alpha}^{-1/4}\bar{L}, \quad x = \hat{\alpha}^{-1/4}\bar{L}\bar{x}, \quad x_m = \hat{\alpha}^{-1/4}\bar{L}\bar{x}_m, \quad \xi = \hat{\alpha}^{-1/4}\bar{L}\bar{\xi}, \\ h = \hat{\alpha}^{1/4}\bar{L}^{-1}\bar{h}, \quad h_m = \hat{\alpha}^{1/4}\bar{L}^{-1}\bar{h}_m, \quad \theta_1 = \hat{\alpha}^{1/2}\bar{L}^{-2}\bar{\theta}_1, \end{gathered} \tag{32}$$

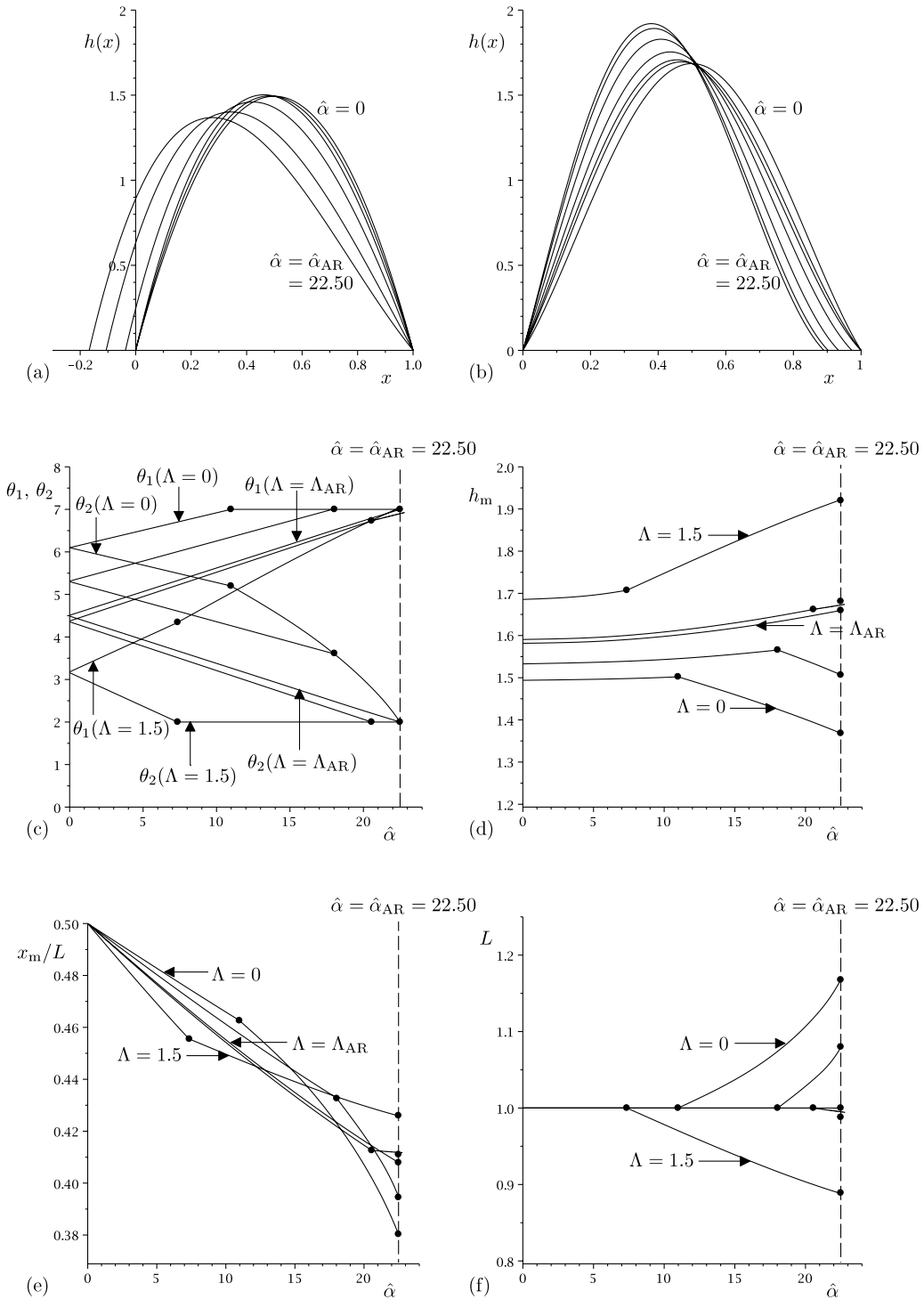

FIG. 10. Plots of (a) the profile of a very wide sessile ridge that first de-pins at its downslope contact line for $\hat{\alpha} = 0$, 5, $\hat{\alpha}_A \simeq 10.99$, 15, 20, $\hat{\alpha}_{AR} = 22.50$ when $\Lambda = 0$ ($< \Lambda_{AR} \simeq 0.93$), $\theta_A = 7$, and $\theta_R = 2$, (b) the profile of a very wide sessile ridge that first de-pins at its upslope contact line for $\hat{\alpha} = 0$, 5, $\hat{\alpha}_R \simeq 7.34$, 10, 15, 20, $\hat{\alpha}_{AR} = 22.50$ when $\Lambda = 1.5$ ($> \Lambda_{AR}$), $\theta_A = 7$, and $\theta_R = 2$, together with plots of (c) the contact angles θ_1 and θ_2, (d) the maximum thickness h_m, (e) the relative location of the maximum thickness x_m/L, and (f) the width L, as functions of $\hat{\alpha}$ for a very wide sessile ridge whose upslope and downslope contact lines de-pin for $\Lambda = 0$, 0.5, $\Lambda_{AR} \simeq 0.93$, 1, 1.5 when $\theta_A = 7$ and $\theta_R = 2$. In (c)–(f) the leftmost dot on each curve indicates the point at which the first contact line (which can be either the upslope or downslope contact line) de-pins, the rightmost dot indicates the point $\hat{\alpha} = \hat{\alpha}_{AR}$ at which the second contact line de-pins, and the vertical dashed line indicates the value $\hat{\alpha} = \hat{\alpha}_{AR} = 22.50$ beyond which there are no steady solutions of the kind considered here.

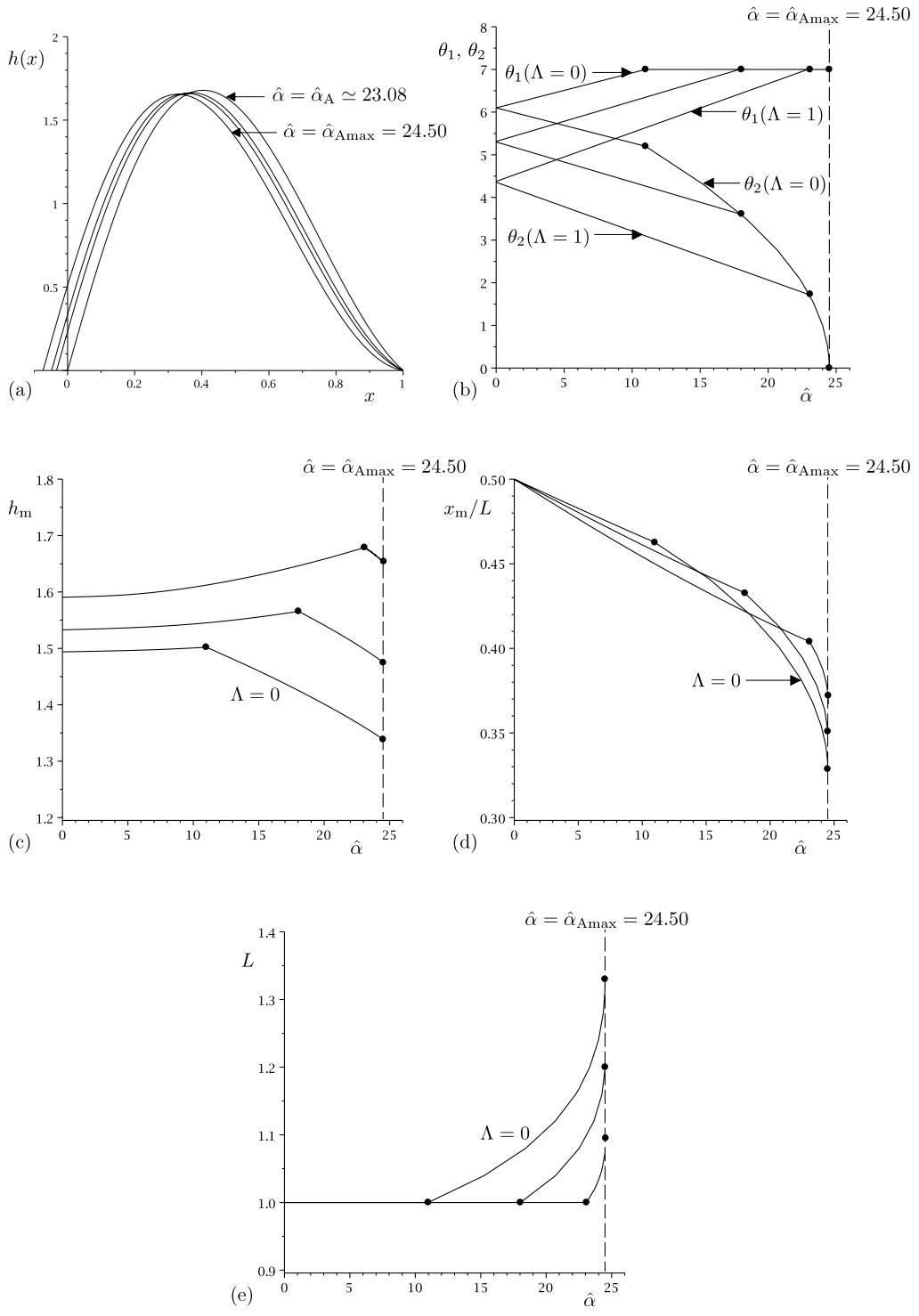

FIG. 11. Plots of (a) the profile of a very wide sessile ridge that has de-pinned at its downslope contact line for $\hat{\alpha} = \hat{\alpha}_{\rm A} \simeq 23.08$, 24, 24.25, $\hat{\alpha}_{\rm Amax} = 24.50$ when $\Lambda = 1$, $\theta_{\rm A} = 7$, and $\theta_{\rm R} = 0$, together with plots of (b) the contact angles θ_1 and θ_2, (c) the maximum thickness $h_{\rm m}$, (d) the relative location of the maximum thickness $x_{\rm m}/L$, and (e) the width L, as functions of $\hat{\alpha}$ for a very wide sessile ridge whose downslope contact line de-pins for $\Lambda = 0$, 0.5, 1 when $\theta_{\rm A} = 7$ and $\theta_{\rm R} = 0$. In (b)–(e) the leftmost dot on each curve indicates the point at which the downslope contact line de-pins, the rightmost dot indicates the point $\hat{\alpha} = \hat{\alpha}_{\rm Amax}$ at which $\theta_2 = 0$, and the vertical dashed line indicates the value $\hat{\alpha} = \hat{\alpha}_{\rm Amax} = 24.50$ beyond which there are no steady solutions of the kind considered here.

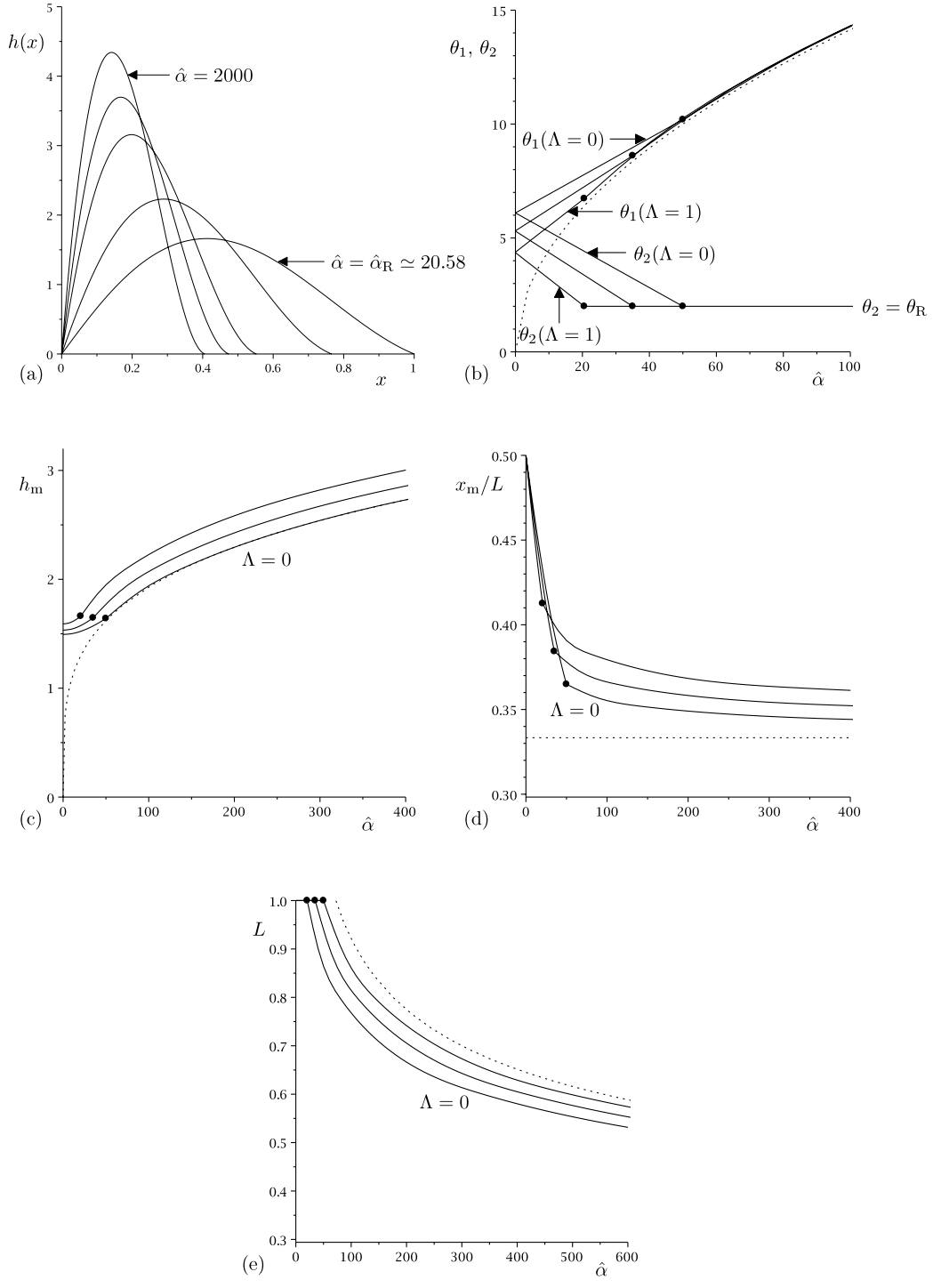

FIG. 12. Plots of (a) the profile of a very wide sessile ridge that has de-pinned at its upslope contact line for $\hat{\alpha} = \hat{\alpha}_R \simeq 20.58$, 100, 500, 1000, 2000 when $\Lambda = 1$, $\theta_A = \infty$, and $\theta_R = 2$, together with plots of (b) the contact angles θ_1 and θ_2, (c) the maximum thickness h_m, (d) the relative location of the maximum thickness x_m/L, and (e) the width L, as functions of $\hat{\alpha}$ for a very wide sessile ridge whose upslope contact line de-pins for $\Lambda = 0$, 0.5, 1 when $\theta_A = \infty$ and $\theta_R = 2$. In (b)–(e) the dots on each curve indicate the point at which the upslope contact line de-pins, and the dotted curves show the leading order asymptotic solutions in the limit of a large angle of inclination of the substrate, $\hat{\alpha} \to \infty$, given by (b) $\theta_1 \simeq 1.41\hat{\alpha}^{1/2} \to \infty$, (c) $h_m \simeq 0.61\hat{\alpha}^{1/4} \to \infty$, (d) $x_m/L \to 1/3^+$, and (e) $L \simeq 2.91\hat{\alpha}^{-1/4} \to 0^+$ for all Λ.

where the leading order scaled width $\bar{L}$ is to be determined as part of the solution. At leading order in the limit $\hat{\alpha} \to \infty$ the effects of the airflow and of the normal component of gravity are negligible, and (12) and (11) become

$$\bar{h}''' - \bar{L}^4 = 0 \tag{33}$$

subject to

$$\bar{h}(0) = 0, \quad \bar{h}(1) = 0, \quad \bar{h}'(1) = 0, \quad \int_0^1 \bar{h}\,\mathrm{d}\bar{x} = V. \tag{34}$$

Equations (33) and (34) have a simple exact solution for the leading order scaled ridge profile, $\bar{h} = \bar{h}(x)$, namely

$$\bar{h} = \frac{\bar{L}^4}{6}\bar{x}(1-\bar{x})^2 = 12V\bar{x}(1-\bar{x})^2, \quad \bar{L} = (72V)^{1/4} \simeq 2.91V^{1/4}, \tag{35}$$

which gives the values

$$\bar{\theta}_1 = \frac{\bar{L}^4}{6} = 12V, \quad \bar{h}_\mathrm{m} = \frac{2\bar{L}^4}{81} = \frac{16V}{9} \simeq 1.78V, \quad \bar{x}_\mathrm{m} = \frac{1}{3}. \tag{36}$$

Figure 13 shows a plot of $\bar{h}(\bar{x})$, and shows that it is skewed downslope with $\bar{x}_\mathrm{m} = 1/3$. The leading order asymptotic solutions for $\theta_1 = (2V\hat{\alpha})^{1/2} \simeq 1.41\hat{\alpha}^{1/2} \to \infty$, $\theta_2 = 0$, $h_\mathrm{m} = (16/9)(V^3\hat{\alpha}/72)^{1/4} \simeq 0.61\hat{\alpha}^{1/4} \to \infty$, $x_\mathrm{m}/L = 1/3$, and $L = (72V/\hat{\alpha})^{1/4} \simeq 2.91\hat{\alpha}^{-1/4} \to 0^+$ are shown with dotted lines in Figures 12(b)–12(e). This asymptotic solution shows how the ridge becomes narrower and thicker and is skewed downslope with larger downslope contact angle in the limit of a large angle of inclination of the substrate. Like the solution in the limit of strong airflow discussed in Sec. IV B, the (scaled) aspect ratio of the ridge in this limit is $O(\hat{\alpha}^{1/2}) \gg 1$, and so while the underlying thin-film approximation will eventually fail when $\hat{\alpha}$ becomes too large, the present asymptotic solution is useful provided that $V \ll \hat{\alpha}^{1/2}V \ll \ell^2$.

VI. A VERY WIDE PENDENT RIDGE

The equation for the profile of a very wide pendent ridge on a nearly horizontal substrate (specifically, when $\pi - \alpha = O(\epsilon)$) differs from the corresponding equation for a very wide sessile ridge (12)

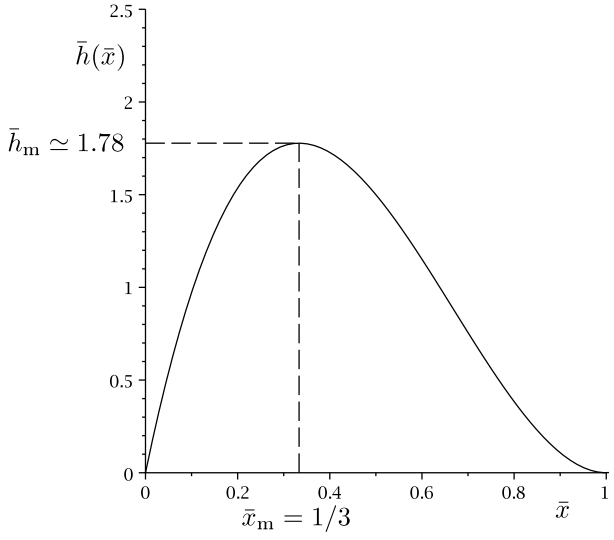

FIG. 13. Plot of the leading order scaled ridge profile $\bar{h}(\bar{x})$ in the limit of a large angle of inclination of the substrate, $\hat{\alpha} \to \infty$, given by (35) and (36).

derived in Sec. III only in the sign of the h' term (i.e., the term corresponding to the normal component of gravity), where Λ is again given by (13) and $\hat{\alpha}$ (≥ 0) is now defined by

$$\hat{\alpha} = \frac{\pi - \alpha}{\epsilon}. \tag{37}$$

This equation is again subject to boundary conditions (11), and (15)–(19) again hold.

The profile in the special case $\Lambda = 0$ can again be obtained from the solution given by Diez *et al.* [Ref. 48, Eq. (5)] and is again given by $H_0 = Vh_0 + \hat{\alpha}h_1$, where the functions $h_0 = h_0(x)$ and $h_1 = h_1(x)$ are now given by

$$h_0 = \frac{\sin\frac{L-x}{2}\sin\frac{x}{2}}{\sin\frac{L}{2} - \frac{L}{2}\cos\frac{L}{2}} \qquad \text{and} \qquad h_1 = x - \frac{L\cos\frac{L-x}{2}\sin\frac{x}{2}}{\sin\frac{L}{2}}, \tag{38}$$

respectively, and θ_1 and θ_2 are again given by (21), where the function $\gamma = \gamma(L)$ is now defined by

$$\gamma = \frac{1}{2}\left(1 - \frac{L}{2}\cot\frac{L}{2}\right)^{-1}. \tag{39}$$

Inspection of (39) reveals that, unlike for a sessile ridge (22), for a pendent ridge γ has multiple branches of solutions. However, γ is a strictly positive, monotonically decreasing function of L in the only interval in which the solutions for h are physically realisable, namely $0 < L < 2\pi$, and satisfies $\gamma \sim 6/L^2 \to \infty$ as $L \to 0^+$ and $\gamma \sim (2\pi - L)/4\pi \to 0^+$ as $L \to 2\pi^-$. In other words, very wide steady pendent ridges are possible only provided that they are not *too* wide. (The closely related problem of the unsteady evolution of thin pendent droplets has been studied in detail by Lister *et al.*[49])

The quasi-static evolution of a very wide pendent ridge as the airflow is gradually strengthened and as the substrate is gradually tilted is similar to that of a very wide sessile ridge described in Secs. IV and V, respectively. For example, Figure 14 shows how θ_1, θ_2, h_m, x_m/L, and L vary with Λ for a range of values of $\hat{\alpha}$ when $\theta_\mathrm{R} = 2$ for both a very wide sessile and a very wide pendent ridge. Figure 14 shows that the behaviour of the two ridges is qualitatively similar, with the pendent ridge (shown with the dashed lines) generally being slightly thicker, de-pinning at a slightly smaller value of Λ_R, and (after de-pinning occurs) being slightly narrower than the corresponding sessile ridge (shown with the solid lines). Moreover, as Figure 14 also shows, at leading order in the limit of a strong airflow, $\Lambda \to \infty$, the effect of gravity is negligible, and both sessile and pendent ridges behave according to the asymptotic solution described in Sec. IV B.

VII. A NARROWER (BUT STILL WIDE) SESSILE OR PENDENT RIDGE

When the substrate is *not* restricted to being nearly horizontal (specifically, when $\alpha = O(1)$), in both sessile and pendent cases the transverse component of gravity is relatively strong and so only a narrower (but still wide) ridge of width much less than the capillary length ℓ can be supported against gravity by capillary and/or external pressure forces. In this case it is appropriate to choose $L_0 = \sqrt{\epsilon}\ell = V^{1/4}\sqrt{\ell}$, so that $\epsilon = V/L_0^2 = \sqrt{V/\ell^2} \ll 1$, the characteristic pressure scale is $\sqrt{\epsilon}\sigma/\ell = \sqrt{\epsilon}\rho g\ell = \rho g V^{1/4}\sqrt{\ell}$, and at leading order in the limit $\epsilon \to 0$ Equation (10) becomes

$$h''' - \sin\alpha + \Lambda\frac{\mathrm{d}}{\mathrm{d}x}\int_0^L \frac{h'(\xi)}{x-\xi}\,\mathrm{d}\xi = 0, \tag{40}$$

where

$$\Lambda = \frac{\rho_\mathrm{a}\sqrt{\epsilon}\ell U_\infty^2}{\pi\sigma} = \frac{\rho_\mathrm{a} V^{1/4}\sqrt{\ell}U_\infty^2}{\pi\sigma}. \tag{41}$$

This equation is again subject to boundary conditions (11), the local behaviour near the contact lines is again given by (15) and (16), the transverse force balance is simply

$$\theta_1^2 - \theta_2^2 = 2V\sin\alpha, \tag{42}$$

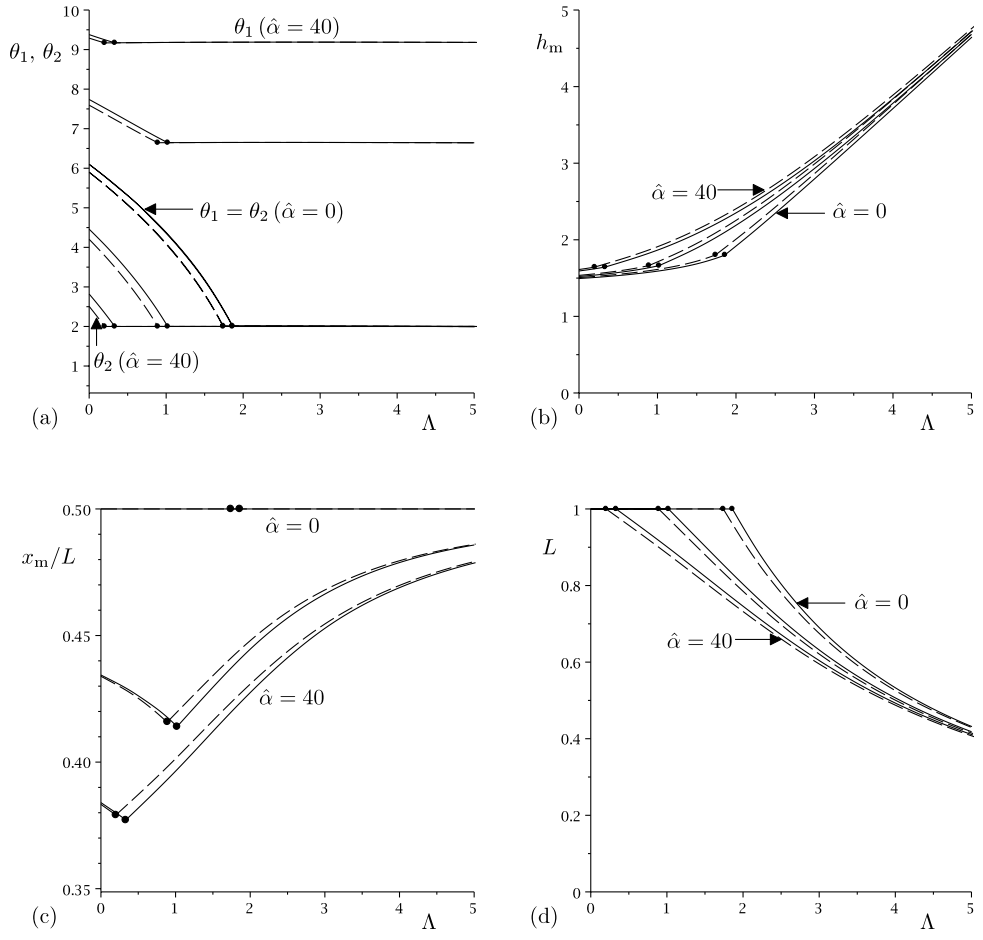

FIG. 14. Plots of (a) the contact angles θ_1 and θ_2, (b) the maximum thickness h_m, (c) the relative location of the maximum thickness x_m/L, and (d) the width L, as functions of Λ for a very wide pendent ridge whose upslope contact line de-pins for $\hat{\alpha} = 0$, 20, 40 when $\theta_R = 2$. The dots indicate the points at which the upslope contact line de-pins (i.e., when $\Lambda = \Lambda_R$ and $\theta = \theta_R$). The solid lines show the results for a very wide sessile ridge for which $\hat{\alpha} = \alpha/\epsilon$ and the dashed lines show the results for a very wide pendent ridge for which $\hat{\alpha} = (\pi - \alpha)/\epsilon$.

and the general form of the solution for the ridge profile is $h = V h_0 + \sin\alpha\, h_1$, where the functions $h_0 = h_0(x)$ and $h_1 = h_1(x)$ again satisfy (19). Comparing (40) with the corresponding equation for a very wide ridge (12) reveals that, as might have been expected, the normal component of gravity is negligible for a narrower ridge, and hence that the leading order solutions for narrower sessile and pendent ridges are identical. Moreover, comparing the definitions of Λ for very wide and narrower ridges (given by (13) and (41), respectively) reveals that the airflow required to support even a narrower ridge on a substrate which is not nearly horizontal is stronger than that required to support a very wide ridge on a nearly horizontal substrate (specifically, U_∞ must be larger by a factor of $\epsilon^{-1/4} = (\ell^2/V)^{1/8} \gg 1$).

The profile in the special case $\Lambda = 0$ was given by Hocking and Miksis [Ref. 50, Eq. (4.2)] and can also be obtained from the solution given by Diez *et al.* [Ref. 48, Eq. (5)] and is given by $H_0 = V h_{00} + \sin\alpha\, h_{01}$, where the functions $h_{00} = h_{00}(x)$ and $h_{01} = h_{01}(x)$ are given by

$$h_{00} = \frac{6x(L-x)}{L^3} \quad \text{and} \quad h_{01} = \frac{x}{12}(L-x)(L-2x), \tag{43}$$

respectively, and θ_1 and θ_2 are given by

$$\theta_{1,2} = \frac{6V}{L^2} \pm \frac{L^2 \sin\alpha}{12}, \tag{44}$$

where again the + sign is taken for θ_1 and the − sign is taken for θ_2. In particular, from (44) it can immediately be deduced that as L is increased both contact angles decrease, just as they do in the case of a very wide ridge discussed in Secs. III–VI. However, since, unlike the value of $\hat{\alpha}$, the value of $\sin\alpha$ cannot exceed unity, unlike in the case of a very wide ridge in which θ_2 always reaches zero for sufficiently large values of L, for a narrower ridge θ_2 reaches zero and θ_1 reaches the non-zero value $\theta_1 = 12V/L^2 = (L^2\sin\alpha)/6$ when $\sin\alpha = 72V/L^4$ only if $72V/L^4 \le 1$ with both θ_1 and θ_2 remaining strictly positive and taking the minimum values $\theta_{1,2} = 6V/L^2 \pm L^2/12$ when $\sin\alpha = 72V/L^4 = 1$ otherwise. In the limit of a weak airflow, $\Lambda \to 0^+$, the ridge profile again takes the form $h = H_0 + \Lambda H_1 + O(\Lambda^2)$, where the leading order term, $H_0 = H_0(x)$, is again simply the solution in the special case $\Lambda = 0$ and the first order term, $H_1 = H_1(x)$, is given by $H_1(x) = Vh_{10} + \sin\alpha\, h_{11}$, where the functions $h_{10} = h_{10}(x)$ and $h_{11} = h_{11}(x)$ are given by

$$h_{10} = \log L - \frac{5x(L-x)}{2L^2} - \frac{x^2(3L-2x)}{L^3}\log x - \frac{(L-x)^2(L+2x)}{L^3}\log(L-x) \tag{45}$$

and

$$h_{11} = \frac{Lx(L-2x)(L-x)}{48} - \frac{x^2(L-x)^2}{24}\log x + \frac{x^2(L-x)^2}{24}\log(L-x), \tag{46}$$

respectively. The behaviours of H_0 and H_1 are qualitatively similar to those in the case of a very wide ridge shown in Figure 2, except that when $72V/L^4 > 1$, $H_0'(L)$ is strictly positive (rather than simply non-negative) and $H_1'(0)$ is strictly negative (rather than simply non-positive).

In general, the behaviour of a narrower ridge can be similar to that of a very wide ridge described in Secs. III–VI, with, as we have already seen, the important qualitative difference that, whereas for a very wide ridge the value of $\hat{\alpha}$ is unbounded, for a narrower ridge the value of $\sin\alpha$ cannot exceed unity, and hence, unlike in the case of a very wide ridge, for a narrower ridge even in the general case in which θ_A is finite and θ_R is non-zero one or both of the contact lines may never de-pin. For example, for a narrower ridge (42) shows that if the second contact line de-pins then it does so when $\sin\alpha = \sin\alpha_{AR}$, where

$$\sin\alpha_{AR} = \frac{\theta_A^2 - \theta_R^2}{2V}, \tag{47}$$

and that if there exists a critical value of Λ for which the two contact lines de-pin simultaneously, denoted again by Λ_{AR}, then the value of Λ relative to Λ_{AR} determines which of the two contact lines de-pins first for increasing $\sin\alpha$. When $\sin\alpha_{AR} = (\theta_A^2 - \theta_R^2)/(2V) \le 1$ this behaviour is qualitatively

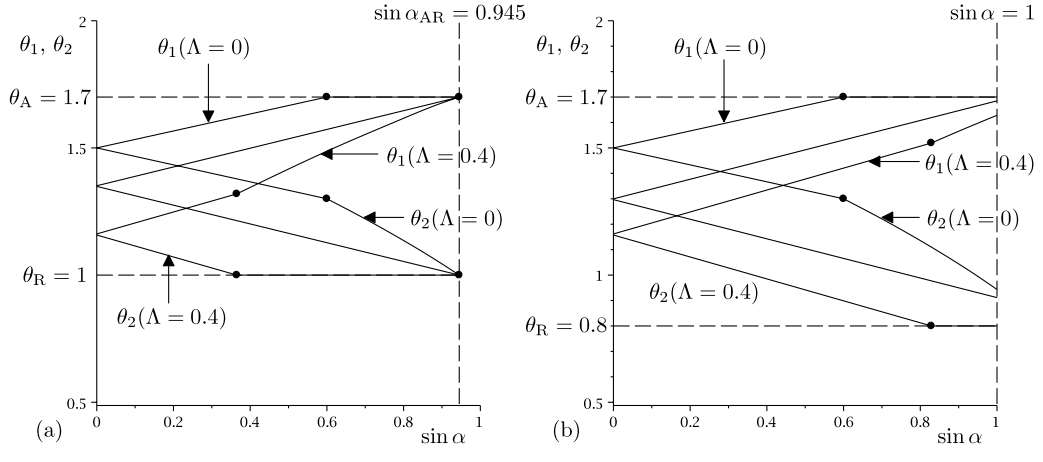

FIG. 15. Plots of the contact angles θ_1 and θ_2 as functions of $\sin\alpha$ for a narrower (but still wide) ridge for (a) $\Lambda = 0$, $\Lambda_{AR} \simeq 0.19$, 0.4 when $L = 2$, $\theta_A = 1.7$, and $\theta_R = 1$ (for which $\sin\alpha_{AR} = (\theta_A^2 - \theta_R^2)/(2V) = 0.945 < 1$), and for (b) $\Lambda = 0$, 0.2, 0.4 when $L = 2$, $\theta_A = 1.7$, and $\theta_R = 0.8$ (for which $(\theta_A^2 - \theta_R^2)/(2V) = 1.125 > 1$). In both (a) and (b), the leftmost dot on each curve indicates the point at which the first contact line (which can be either the upslope or the downslope contact line) de-pins, and in (b) the rightmost dot indicates the point $\sin\alpha = \sin\alpha_{AR} = 0.945$ at which the second contact line de-pins.

the same as in the case of a very wide ridge discussed in Sec. V B. However, when $(\theta_A^2 - \theta_R^2)/(2V) > 1$ the second contact line never de-pins. This behaviour is illustrated in Figure 15 which shows how θ_1 and θ_2 vary with $\sin\alpha$ for a range of values of Λ. Specifically, Figure 15(a) shows the behaviour in the case $L = 2$, $\theta_A = 1.7$, and $\theta_R = 1$ in which $\sin\alpha_{AR} = (1.7^2 - 1)/(2V) = 0.945 < 1$, $\Lambda_{AR} \simeq 0.19$, and the behaviour is qualitatively the same as that in the case of a very wide sessile ridge shown in Figure 10, while Figure 15(b) shows the behaviour in the case $L = 2$, $\theta_A = 1.7$ and $\theta_R = 0.8$ in which $(1.7^2 - 0.8^2)/(2V) = 1.125 > 1$, Λ_{AR} does not exist, and the second contact line never de-pins. Closer inspection of Figure 15(b) reveals that for values of Λ less than that at which $\theta_1 = \theta_A$ at $\sin\alpha = 1$ (exemplified by the case $\Lambda = 0$) only the downslope contact line de-pins, for values of Λ greater than that at which $\theta_2 = \theta_R$ at $\sin\alpha = 1$ (exemplified by the case $\Lambda = 0.4$) only the upslope contact line de-pins, while for intermediate values of Λ (exemplified by the case $\Lambda = 0.2$) neither contact line ever de-pins.

VIII. SUMMARY AND CONCLUSIONS

In the present work we described the behaviour of a steady thin sessile or pendent ridge of fluid on an inclined planar substrate which is strongly coupled to the external pressure gradient arising from an inviscid airflow parallel to the substrate far from the ridge. When the substrate is nearly horizontal (specifically, when $\alpha = O(\epsilon)$ for a sessile ridge or $\pi - \alpha = O(\epsilon)$ for a pendent ridge), a very wide ridge can be supported against gravity by capillary and/or external pressure forces, whereas when the substrate is not restricted to being nearly horizontal (specifically, when $\alpha = O(1)$) only a narrower (but still wide) ridge can be supported. Classical thin-aerofoil theory was adapted to obtain the governing singular integro-differential equation for the profile of the ridge in each case. Attention focused mainly on the case of a very wide sessile ridge. In Sec. III we described some basic properties of the solution, while in Secs. IV and V we used a combination of numerical and asymptotic techniques to analyse the effect of varying the strength of the airflow, Λ, and the angle of inclination of the substrate, $\hat{\alpha}$, respectively.

In Sec. IV A we studied a pinned ridge for increasing Λ and showed that the effect of strengthening the airflow is to push the ridge down near to its edges and to pull it up near to its middle. In Sec. IV B we showed that at a critical value of $\Lambda = \Lambda_R$ the upslope contact angle reaches the receding contact angle θ_R at which the upslope contact line de-pins, and continuing to increase Λ beyond Λ_R results in the de-pinned ridge becoming narrower, thicker, and closer to being symmetric in the limit of a strong airflow, $\Lambda \to \infty$.

In Sec. V A we studied a pinned ridge for increasing $\hat{\alpha}$ and showed that the effect of tilting the substrate is to skew the ridge downslope. In Sec. V B we showed that, depending on the values of the advancing and receding contact angles, the ridge may first de-pin at either the upslope or the downslope contact line but, in general, eventually both contact lines de-pin at $\hat{\alpha} = \hat{\alpha}_{AR} = (\theta_A^2 - \theta_R^2)/(2V)$. In Secs. V C and V D we considered the special cases $\theta_R = 0$, in which only the downslope contact line de-pins, and $\theta_A = \infty$, in which only the upslope contact line de-pins, respectively.

In Sec. VI we showed that the behaviour of a very wide pendent ridge is qualitatively similar to that of a very wide sessile ridge, while in Sec. VII we showed that the important qualitative difference between the behaviour of a very wide ridge and a narrower ridge is that for the latter even in the general case in which θ_A is finite and θ_R is non-zero, one or both of the contact lines may never de-pin.

Since the present work was concerned solely with a steady ridge, the natural next step should be to analyse the stability of such ridges to both linear and non-linear perturbations, following the approaches pioneered by Hocking,[51] Hocking and Miksis,[50] King *et al.*,[52] and Diez *et al.*[48,53] for ridges in the absence of an airflow, and the unsteady evolution of a ridge, perhaps following the approach of Lister *et al.*[49] for droplets in the absence of an airflow.

The goal of the present work was to adapt thin-aerofoil theory to analyse a situation in which the profile of the ridge and the airflow is strongly coupled. This semi-analytical approach naturally complements the considerable body of work using numerical methods. As we have seen, the great advantage of this approach is that it leads to a relatively simple integro-differential equation for the profile of the ridge which, since it is amenable to both numerical and asymptotic analyses, enables

us to obtain a complete description of the behaviour and, in particular, to make predictions for the deformation and possible de-pinning of the ridge involving only a small number of non-dimensional parameters. Moreover, the present approach could be made more realistic by extending it in several directions, such as to include detachment of the airflow at some point on the free surface of the ridge (as discussed by, for example, Durbin[25]), a non-zero transverse shear stress at the free surface of the ridge (as discussed by, for example, King and Tuck[26] and Sullivan *et al.*[24]), and/or the effect of substrate topography (as discussed by, for example, Sommers *et al.*[54] and Hu *et al.*[55]).

ACKNOWLEDGMENTS

The first author (C.P.) gratefully acknowledges the financial support of the University of Strathclyde via a Postgraduate Research Scholarship. All three authors gratefully acknowledge valuable discussions about the rain–wind-induced vibrations of cables and related problems with Dr. Ian J. Taylor and Mr. (now Dr.) Andrew C. Robertson (Department of Mechanical Engineering, University of Strathclyde). This work was begun while the second author (S.K.W.) was a Visiting Fellow in the Oxford Centre for Collaborative Applied Mathematics (OCCAM), Mathematical Institute, University of Oxford, United Kingdom, and completed while he was a Visiting Fellow at the Isaac Newton Institute for Mathematical Sciences in Cambridge, United Kingdom as part of the programme on "Mathematical Modelling and Analysis of Complex Fluids and Active Media in Evolving Domains" and a Leverhulme Trust Research Fellow supported by Award No. RF-2013-355 "Small Particles, Big Problems: Understanding the Complex Behaviour of Nanofluids." This publication was based on work supported in part by Award No. KUK-C1-013-04, made by King Abdullah University of Science and Technology (KAUST).

[1] J. Fan, M. C. T. Wilson, and N. Kapur, "Displacement of liquid droplets on a surface by a shearing air flow," J. Colloid Interface Sci. **356**, 286 (2011).
[2] A. C. Robertson, I. J. Taylor, S. K. Wilson, B. R. Duffy, and J. M. Sullivan, "Numerical simulation of rivulet evolution on a horizontal cable subject to an external aerodynamic field," J. Fluids Struct. **26**, 50 (2010).
[3] C. Lemaitre, E. de Langre, and P. Hémon, "Rainwater rivulets running on a stay cable subject to wind," Eur. J. Mech., B: Fluids **29**, 251 (2010).
[4] H. Kim, S. Grobe, G. E. Elsinga, and J. Westerweel, "Full 3D-3C velocity measurement inside a liquid immersion droplet," Exp. Fluids **51**, 395 (2011).
[5] J. A. Cuminato, A. D. Fitt, M. J. S. Mphaka, and A. Nagamine, "A singular integro-differential equation model for dryout in LMFBR boiler tubes," IMA J. Appl. Math. **75**, 269 (2010).
[6] F.-C. Chou and P.-Y. Wu, "Effect of air shear on film planarization during spin coating," J. Electrochem. Soc. **147**, 699 (2000).
[7] T. G. Myers and J. P. F. Charpin, "A mathematical model for atmospheric ice accretion and water flow on a cold surface," Int. J. Heat Mass Transfer **47**, 5483 (2004).
[8] X. Li and C. Pozrikidis, "Shear flow over a liquid drop adhering to a solid surface," J. Fluid Mech. **307**, 167 (1996).
[9] P. Dimitrakopoulos and J. J. L. Higdon, "Displacement of fluid droplets from solid surfaces in low-Reynolds-number shear flows," J. Fluid Mech. **336**, 351 (1997).
[10] P. Dimitrakopoulos and J. J. L. Higdon, "On the displacement of three-dimensional fluid droplets from solid surfaces in low-Reynolds-number shear flows," J. Fluid Mech. **377**, 189 (1998).
[11] P. Dimitrakopoulos and J. J. L. Higdon, "On the gravitational displacement of three-dimensional fluid droplets from inclined solid surfaces," J. Fluid Mech. **395**, 181 (1999).
[12] P. Dimitrakopoulos and J. J. L. Higdon, "On the displacement of three-dimensional fluid droplets adhering to a plane wall in viscous pressure-driven flows," J. Fluid Mech. **435**, 327 (2001).
[13] A. D. Schleizer and R. T. Bonnecaze, "Displacement of a two-dimensional immiscible droplet adhering to a wall in shear and pressure-driven flows," J. Fluid Mech. **383**, 29 (1999).
[14] S. Yon and C. Pozrikidis, "Deformation of a liquid drop adhering to a plane wall: Significance of the drop viscosity and the effect of an insoluble surfactant," Phys. Fluids **11**, 1297 (1999).
[15] P. D. M. Spelt, "Shear flow past two-dimensional droplets pinned or moving on an adhering channel wall at moderate Reynolds numbers: A numerical study," J. Fluid Mech. **561**, 439 (2006).
[16] J. Zhang, M. J. Miksis, and S. G. Bankoff, "Nonlinear dynamics of a two-dimensional viscous drop under shear flow," Phys. Fluids **18**, 072106 (2006).
[17] P. Dimitrakopoulos, "Deformation of a droplet adhering to a solid surface in shear flow: Onset of interfacial sliding," J. Fluid Mech. **580**, 451 (2007).
[18] P. Dimitrakopoulos, "Gravitational effects on the deformation of a droplet adhering to a horizontal solid surface in shear flow," Phys. Fluids **19**, 122105 (2007).
[19] H. Ding and P. D. M. Spelt, "Onset of motion of a three-dimensional droplet on a wall in shear flow at moderate Reynolds numbers," J. Fluid Mech. **599**, 341 (2008).
[20] E. Shirani and S. Masoomi, "Deformation of a droplet in a channel flow," J. Fuel Cell Sci. Technol. **5**, 041008 (2008).

[21] K. Sugiyama and M. Sbragaglia, "Linear shear flow past a hemispherical droplet adhering to a solid surface," J. Eng. Math. **62**, 35 (2008).
[22] H. Ding, M. N. H. Gilani, and P. D. M. Spelt, "Sliding, pinch-off and detachment of a droplet on a wall in a shear flow," J. Fluid Mech. **644**, 217 (2010).
[23] L. Hao and P. Cheng, "An analytical model for micro-droplet steady movement on the hydrophobic wall of a micro-channel," Int. J. Heat Mass Transfer **53**, 1243 (2010).
[24] J. M. Sullivan, C. Paterson, S. K. Wilson, and B. R. Duffy, "A thin rivulet or ridge subject to a uniform transverse shear stress at its free surface due to an external airflow," Phys. Fluids **24**, 082109 (2012).
[25] P. A. Durbin, "On the wind force needed to dislodge a drop adhered to a surface," J. Fluid Mech. **196**, 205 (1988).
[26] A. C. King and E. O. Tuck, "Thin liquid layers supported by steady air-flow surface traction," J. Fluid Mech. **251**, 709 (1993).
[27] A. C. King, E. O. Tuck, and J.-M. Vanden-Broeck, "Air-blown waves on thin viscous sheets," Phys. Fluids A **5**, 973 (1993).
[28] J. A. Cuminato, A. D. Fitt, and S. McKee, "A review of linear and nonlinear Cauchy singular integral and integro-differential equations arising in mechanics," J. Integr. Equations Appl. **19**, 163 (2007).
[29] J. A. Moriarty, L. W. Schwartz, and E. O. Tuck, "Unsteady spreading of thin liquid films with small surface tension," Phys. Fluids A **3**, 733 (1991).
[30] J. J. Kriegsmann, M. J. Miksis, and J.-M. Vanden-Broeck, "Pressure driven disturbances on a thin viscous film," Phys. Fluids **10**, 1249 (1998).
[31] I. S. McKinley, S. K. Wilson, and B. R. Duffy, "Spin coating and air-jet blowing of thin viscous drops," Phys. Fluids **11**, 30 (1999).
[32] T. G. Myers, H. X. Liang, and B. Wetton, "The stability and flow of a rivulet driven by interfacial shear and gravity," Int. J. Nonlinear Mech. **39**, 1239 (2004).
[33] H. H. Saber and M. S. El-Genk, "On the breakup of a thin liquid film subject to interfacial shear," J. Fluid Mech. **500**, 113 (2004).
[34] M. Villegas-Díaz, H. Power, and D. S. Riley, "Analytical and numerical studies of the stability of thin-film rimming flow subject to surface shear," J. Fluid Mech. **541**, 317 (2005).
[35] S. K. Wilson and B. R. Duffy, "Unidirectional flow of a thin rivulet on a vertical substrate subject to a prescribed uniform shear stress at its free surface," Phys. Fluids **17**, 108105 (2005).
[36] N. H. Shuaib, H. Power, S. Hibberd, and K. Simmons, "A numerical study of wave structures developed on the free surface of a film flowing on inclined planes and subjected to surface shear," Int. J. Numer. Methods Eng. **68**, 755 (2006).
[37] N. Alleborn, A. Sharma, and A. Delgado, "Probing of thin slipping films by persistent external disturbances," Can. J. Chem. Eng. **85**, 586 (2007).
[38] J. P. Pascal and S. J. D. D'Alessio, "Instability of power-law fluid flows down an incline subjected to wind stress," Appl. Math. Modell. **31**, 1229 (2007).
[39] J. M. Sullivan, S. K. Wilson, and B. R. Duffy, "A thin rivulet of perfectly wetting fluid subject to a longitudinal surface shear stress," Q. J. Mech. Appl. Math. **61**, 25 (2008).
[40] S. K. Wilson, J. M. Sullivan, and B. R. Duffy, "The energetics of the breakup of a sheet and of a rivulet on a vertical substrate in the presence of a uniform surface shear stress," J. Fluid Mech. **674**, 281 (2011).
[41] Y. M. Yatim, B. R. Duffy, and S. K. Wilson, "Similarity solutions for unsteady shear-stress-driven flow of Newtonian and power-law fluids: Slender rivulets and dry patches," J. Eng. Math. **73**, 53 (2012).
[42] C. W. J. Berendsen, J. C. H. Zeegers, and A. A. Darhuber, "Thinning and rupture of liquid films by moving slot jets," Langmuir **29**, 15851 (2013).
[43] C. Paterson, S. K. Wilson, and B. R. Duffy, "Rivulet flow round a horizontal cylinder subject to a uniform surface shear stress," Q. J. Mech. Appl. Math. **67**, 567 (2014).
[44] M. Van Dyke, *Perturbation Methods in Fluid Mechanics*, 2nd ed. (Parabolic, 1975).
[45] C. Paterson, "Thin fluid films subject to external airflows," Ph.D. thesis, University of Strathclyde, Glasgow, 2013.
[46] E. B. Dussan V, "On the ability of drops to stick to surfaces of solids. Part 3. The influences of the motion of the surrounding fluid on dislodging drops," J. Fluid Mech. **174**, 381 (1987).
[47] T. D. Blake and K. J. Ruschak, "Wetting: Static and dynamic contact lines," in *Liquid Film Coating*, edited by S. F. Kistler and P. M. Schweizer (Chapman and Hall, 1997).
[48] J. A. Diez, A. G. González, and L. Kondic, "Instability of a transverse liquid rivulet on an inclined plane," Phys. Fluids **24**, 032104 (2012).
[49] J. R. Lister, J. M. Rallison, and S. J. Rees, "The nonlinear dynamics of pendent drops on a thin film coating the underside of a ceiling," J. Fluid Mech. **647**, 239 (2010).
[50] L. M. Hocking and M. J. Miksis, "Stability of a ridge of fluid," J. Fluid Mech. **247**, 157 (1993).
[51] L. M. Hocking, "Spreading and instability of a viscous fluid sheet," J. Fluid Mech. **211**, 373 (1990).
[52] J. R. King, A. Münch, and B. Wagner, "Linear stability of a ridge," Nonlinearity **19**, 2813 (2006).
[53] J. A. Diez, A. G. González, and L. Kondic, "On the breakup of fluid rivulets," Phys. Fluids **21**, 082105 (2009).
[54] A. D. Sommers, J. Ying, and K. F. Eid, "Predicting the onset of condensate droplet departure from a vertical surface due to air flow – Applications to topographically-modified, micro-grooved surfaces," Exp. Therm. Fluid Sci. **40**, 38 (2012).
[55] H. Hu, S. Huang, and L. Chen, "Displacement of liquid droplets on micro-grooved surfaces with air flow," Exp. Therm. Fluid Sci. **49**, 86 (2013).